Compact Multi-Wideband Array for Millimeter-Wave Communications Using Squint Beams

XIAOLIANG PAN, **CHUNGUO LI**, (Senior Member, IEEE),
MENG HUA, (Student Member, IEEE), **WEN YAN**, (Member, IEEE),
AND LUXI YANG, (Senior Member, IEEE)

School of Information Science and Engineering, Southeast University, Nanjing 210096, China

Corresponding author: Luxi Yang (lxyang@seu.edu.cn)

ABSTRACT Millimeter-wave (mmWave) cellular systems leverage the hybrid analog-digital structure to balance the costs and the capacity performance by using fewer Radio Frequency (RF) chains and the spatial sparsity of the channel. Besides, a more broadband system is the natural outgrowth of the gigantic frequency resource in mmWave band. However, it becomes precarious when the hybrid structure is extended to the wideband systems as the wideband phase shifters are used in the array. In this article, a multi-wideband planar array structure using the concept of Sierpinski carpet fractal is proposed, which exploits the beam squinting property instead of forming several independent beams through an existing hybrid structure. Moreover, multi-subarray can form a larger antenna array without additional costs of phase shifters for the wider range of values. First, we derive several properties of the steering beams from a wideband linear array. Then, we exploit the beam squinting property of the planar arrays employing wideband ideal phase shifters to form multi-beam. The functionality of the phase shifters in an array is simplified by a set of wideband cells connected in series. The maximum cell number needed in the array is derived, and during this derivation, we find a flaw of the beam squinting method. Finally, we present numerical results on the performance of the proposed arrays with the proposed algorithm, based on a cellular scenario of one base station (BS) and multi-user, where the BS has four subarrays and each user has one subarray.

INDEX TERMS Millimeter-wave, wideband antenna array, wideband phase shifter, beam squinting, Sierpinski carpet.

I. INTRODUCTION

In millimeter-wave (mmWave) cellular systems, how to take full advantage of the spatial sparsity of the mmWave channel and the vast amount of frequency resources in the mmWave band is an open problem [1]–[3]. For a conventional system, there are three principal antenna array configurations: analog, digital, and hybrid respectively [4], [5]. The analog beamforming structure, known as phased array, has been widely applied in electronically scanned radar systems over the past few decades. With the development of multiple-input multiple-output (MIMO) array [6] and large-scale array [7], [8], digital beamforming structure is

used to flexibly harmonize the amplitude and direction of the main beam and sidelobes [9], without considering the costs and power consumption of the mmWave array. By exploiting the sparse nature of the mmWave channels, more reasonable multi-beam antenna arrays [10], [11], hybrid analog-digital structures have been proposed [12], [13]. The two suggested hybrid architectures in mmWave systems of today are (i) array of phased subarrays, and (ii) array of a fully-connected array. Option (i) suffers from the very limited field-of-view and formation of grating lobes, while (ii) is terrible in terms of efficiency due to Radio Frequency (RF) combination losses and RF complexity.

For the fully connected hybrid structure that can be interpreted as a fully connected multi-beam analog array [14] with extra processing capability in the digital domain, the number

---

The associate editor coordinating the review of this manuscript and approving it for publication was Giorgio Montisci.

of the RF chains is usually no more than the number of antennas and no less than the number of the signal streams in the baseband [13]. Arguably, this hybrid structure can provide at most as many effective beams as the number of RF chains. More recently, the work in [15]–[19] tries to transmit more signal streams than the number of RF chains, even transmitting one more signal stream than the number of RF chains with a complicated design [18] is challenging and encouraging. On the other hand, the work in [12], [17], [20] considers imitating digital domain beamforming in the RF domain, using twice as many RF chains as the number of signal streams [12], and even further paralleling two phase shifters to the RF chain of an antenna to save the number of RF chains [17], [20]. Although combining two phase shifters in the RF domain to simulate the digital processing by varying the amplitude and phase of the signal is relatively novel, it relies on the range of continuous values of the phase shifter and its refresh rate [17]. In fact, this violates the original design intent of a phase shifter and may require the design of more specialized RF components.

The hybrid structure is promising for the fact that the RF chain is much more expensive than the phase shifter, that the mmWave RF chain consumes excessive power, and that the large-scale antenna array is a trend for mmWave systems. When it comes to the wideband, as the abundant frequency resources in the mmWave band, the RF chain and phase shifter are more expensive and more power consuming than the corresponding narrowband components. So the wideband hybrid structure should be streamlined to some extent.

On the other hand, antenna arrays encounter new challenges in wideband scenarios, namely, the assumption of half-wavelength spacing between array elements is not suitable for very wide bandwidths directly. Fractal antennas have been an active research interest, due to their compact size, frequency-independent multi-band nature [21], and ability to realizing thinning or low sidelobe beams. It has two main areas [22]–[24]: (i) design of individual fractal shaped antenna elements, and (ii) design of antenna arrays that exploit the fractal concepts. The first approach has been extensively studied, such as using Sierpinski triangle [25] and Sierpinski carpet [26], or even combining several fractal structures in one antenna [27]. While the design methods and advantages of the second way are still being explored and developed [22].

In the literature on wideband hybrid precoding, a number of efforts are based on the OFDM-based structure, with multi-sub-frequency baseband precoders and a uniform RF precoder for each RF chain [28]–[30]. However, the unified RF precoder implies the use of ideal phase shifters, which will inevitably result in beam squinting [31]. This will degrade the performance of beam-based systems, and the feasibility of OFDM-based systems can be an issue for very wideband systems. Some work has paid attention to the effect of beam squint [32]–[39], fixing it in the digital domain [40], with codebooks [41], or utilizing the ideal time delay phase shifters [42]–[45].

However, the harnessing of beam squinting to generate independent multi-beam is unexplored in the literature. With squint beams, it is also possible to serve multi-user with just one wideband RF chain, with one individual signal stream for each user. Meanwhile, the hybrid beamforming structure should adapt to the new situation, the enhanced analog structure with one wideband RF chain and wideband phase shifters is one option, it also keeps the baseband processing ability for multi-data-stream with multi-sub-frequency. Moreover, thanks to the subarrays structure with multi-RF-chain in each subarray [46], this kind of structure is easy to extend to a large wideband antenna array with one RF chain each subarray.

While from the perspective of cost-saving, the function of phases shifters in the array could be achieved by a group of wideband cells [47], which could be recognized as an implementation for finite resolution phase shifters (FRPS) [48]–[50] while with non-integers quantization bits. Moreover, the time modulated array (TMA) [51] can produce a virtual phase shifter for each antenna in the array. For these virtual phase shifters are not true time delays (TTDs), beam squinting is also achieving.

In this article, we investigate wideband antenna arrays that employ spatial squint beams for cellular communications. Our research is based on overly idealistic assumptions and is in its infancy, both the non-isotropic pattern and the mutual coupling of the array elements should be considered for implementing a realistic antenna array [52]. The main contributions of the paper can be summarized as follows:

- We design a compact multi-band ultra-wideband planar array structure for mmWave communication, using the Sierpinski carpet topology and the beam squinting property to serve multi-user.
- We utilize a group of cells to implement the functionality of the phase shifter in the array and give a derivation of the number of cells required for the planar array.
- We reveal that the squint beams cannot cover all angles of the hemisphere through the planar array when determining the value of the phase shifters in the array.
- We use multi-subarray to form a larger array which further cuts the number of cells of the larger array by compensating for the phase difference of the subarrays in the digital domain.
- We validate the usage of the proposed array with simulations in a multi-user scenario, where the proposed algorithm calculates the number of cells of the virtual phase shifters and the working frequencies of the steering beams for the users.

The rest of the paper is organized as follows. In Section II, we present the beam property of the narrowband array and derive the beam property for the wideband array. In Section III, we present a multi-wideband planar array structure with the Sierpinski carpet fractal. In Section IV, we derive the cell number needed in the planar array, where we reveal that this array can only change the vertical angle of the steer main beam direction with beam squinting. In Section V, we present a scenario of one base station (BS)

and multi-user, where the BS is with a big array composed of four subarrays and each user is with one subarray, we give the algorithm manifesting the usage of the proposed array in this scenario. In Section VI, simulation results showing the performance of the proposed algorithm for the proposed array, before concluding the paper in Section VII.

The following notations are adopted throughout this article: Boldface uppercase letters, boldface lowercase letters, and lowercase letters are used to denote matrices, vectors and scalars, respectively; The superscripts $(\cdot)^T$, $(\cdot)^*$, $(\cdot)^H$ denote the transpose, conjugate and conjugate transpose respectively; $\| \cdot \|_F$ represents the Frobenius norm of a matrix; $\mathbf{I}_N$ is the $N \times N$ identity matrix; $\otimes$, $\odot$ and $*$ represent Kronecker, Khatri-Rao and Hadamard matrix products, respectively; $vec(\cdot)$ indicates vectorization; $\{\cdot\}_{mn}$ is the element at m^{th} row and n^{th} column of a matrix; $\lfloor \cdot \rfloor$ and $\lceil \cdot \rceil$ denote floor and ceiling function, respectively; $| \cdot |$ is the amplitude of a complex value.

II. WIDEBAND PHASE SHIFTER AND BEAMFORMING

Phase shifters are microwave network modules that can change the phase of incident RF signals [53]. A phase shifter with value φ is denoted by $e^{j\varphi}$ or $e^{-j\varphi}$.

On the one hand, the time delay property of the Fourier transform (FT) pair $x(t) \longleftrightarrow X(j\omega)$ is

$$x(t - \tau_0) \longleftrightarrow X(j\omega)e^{-j\omega\tau_0}. \tag{1}$$

From (1), adding a phase shifter with value $\varphi = \omega\tau_0$ to an antenna in the RF domain can be regarded as multiplying $e^{-j\omega\tau_0}$ in the frequency domain, which results in a delay τ_0 in the time domain of the transmitted signal.

On the other hand, while $e^{-j\varphi}$ is well suited to represent the phase shifter of value φ corresponding to an array antenna when transmitting a beam, it is more appropriate to use $e^{j\varphi}$ to represent this phase shifter for a receiving beam, due to the fact that in this case the direction of the delay is from the antenna to the baseband of the array, which is opposite to the direction of the delay when transmitting a beam.

For narrowband systems, the phase shifter and the time delay have the same effect. At a particular working frequency f_c, the phase shifter with value φ has a deterministic time delay τ, from (1) yields $\varphi = 2\pi f_c \tau$. In wideband scenarios, the expression for a phase shifter or a time delay module at frequency f_i can be written as

$$\varphi_i = 2\pi f_i \tau_i, \tag{2}$$

where the beam of the array with the true time delays and the array with the ideal phase shifters have different properties, which will be elaborated in the following subsections.

A. THE FUNDAMENTALS OF NARROWBAND ARRAY BEAMFORMING

Formula derivations for both beam direction and beamwidth could be found in [54, chap.6], [55, chap.2], which can be easily extended to wideband array scenarios. We will illuminate this with a linear antenna array in this subsection. In addition,

we will take care of the required attributes of planar arrays when needed in Section IV.

For a uniform linear array of N identical elements, the radiated field E_t of the far field can be written as the product of the radiation pattern of a single reference element and the array factor (AF) of the array as $\mathrm{E}_t = \mathrm{E}_{ref} \times \mathrm{AF}$.

According to (6-10) in [54], when the first element of an array is chosen as a reference, the AF can be written as

$$\mathrm{AF} = \frac{\sin\left(\frac{N}{2}\psi\right)}{\sin\left(\frac{1}{2}\psi\right)} e^{j(N-1)\psi/2}. \tag{3}$$

On the other hand, from (6-10a) in [54], if the center point of the array is chosen as a reference, the AF is then given by

$$\mathrm{AF} = \frac{\sin\left(\frac{N}{2}\psi\right)}{\sin\left(\frac{1}{2}\psi\right)}, \tag{4}$$

where ψ is the total progressive phase difference of a transmitting array in any direction θ, which can be written as [1]

$$\psi = kd\sin\theta - \beta, \tag{5}$$

where $k = 2\pi f/c$ is the free space wavenumber, f is the operating frequency, c is the velocity of electromagnetic wave, θ is the angle between the main beam direction and the broadside, as showing in Fig. 1, d and β are the element spacing and the phase excitation difference between elements, respectively. When a uniformly spaced array using analog phase shifters employs beam steering, β is the progressive phase shifter difference between adjacent antenna elements.
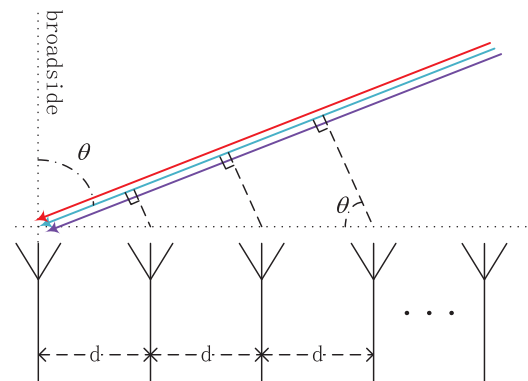

FIGURE 1. A linear array with wideband incident beams.

Notice from (3) and (4) that the reference point in the array does not change the amplitude of AF. If we choose

---

[1]We substitute (5) for $\psi = kd\sin\theta + \beta$ in [54] with the following reasons: a) it is easier to understand when the phase shifter is positive; b) ψ remains unchanged for both writings; c) the phase-shifting array response vector can then be expressed by replacing $kd\sin\theta$ of the array response vector in [28] with β; d) the formula for AF can then be used to put the channel model and the beam steering vector together for interpretation. If the channel has a path with a departure angle of θ_1, an arrival angle of ϕ_1, a path coefficient α_1, and steering phase shifter vectors of progressive differences β_t and β_r for the transmit and receive arrays, respectively, then the equivalent baseband power gain of this channel path is $|\alpha_1 \mathrm{AF}_{r1} \mathrm{AF}_{t1}|^2$, where the AFs at the transmitting and receiving sides are $\mathrm{AF}_{t1} = \mathbf{a}(\theta_1)^H \mathbf{a}(\beta_t)$ and $\mathrm{AF}_{r1} = \mathbf{a}(\beta_r)^H \mathbf{a}(\phi_1)$. $\mathbf{a}$ is the array manifold vector for linear arrays, which we will deal with later in this article.

the first antenna as the reference with a phase-shifting value $\varphi_0 = 0$, then the value of the phase shifter connecting to the nth antenna is $\varphi_{n-1} = (n-1)\beta$. And in (3), $\mathrm{AF}(\psi) \neq \mathrm{AF}(-\psi)$.

The AF in (4) can be written in normalized form as

$$(\mathrm{AF})_n = \frac{1}{N}\left[\frac{\sin\left(\frac{N}{2}\psi\right)}{\sin\left(\frac{1}{2}\psi\right)}\right]. \tag{6}$$

From (6), the AF reaches its normalized extreme values of 1 as it reduces to the 0/0 form when

$$\frac{1}{2}\psi = \pm m\pi, \quad m = 0, 1, 2, \cdots. \tag{7}$$

When $d \leq \frac{\lambda}{2}$, (7) has a solution for θ only if m=0. If $m = 1, 2, \cdots$, there is no solution for θ in $|\sin\theta| > 1$. Here λ is the wavelength. In addition, grating lobes appear when $d > \frac{\lambda}{2}$. This phenomenon can be explained by (7) because $\sin\theta = \frac{\beta \pm 2\pi m}{kd}$ may have other solutions for θ when $m = 1, 2, \cdots$.

Regardless of the ratio of antenna spacing d to working wavelength λ, the main beam direction of this array is always

$$\theta_m = \arcsin\frac{\beta}{kd}. \tag{8}$$

When ψ is small, such as in the mainlobe, (6) can be approximated by

$$(\mathrm{AF})_n \approx \left[\frac{\sin\left(\frac{N}{2}\psi\right)}{\left(\frac{N}{2}\psi\right)}\right]. \tag{9}$$

The 3 dB direction of the main beam θ_h can be found by $(\mathrm{AF})_n = \sqrt{0.5}$, namely when $\frac{\sin x}{x} = \sqrt{0.5}$, $x \approx \pm 1.391$, θ_h in (5) can be approximated by

$$\theta_h \approx \arcsin\left[\frac{1}{kd}\left(\beta \pm \frac{2.782}{N}\right)\right], \tag{10}$$

and the half-power beamwidth (HPBW) Θ_h can be calculated by $\Theta_h \approx 2\left|\theta_m - \theta_h\right|$.

In addition, the direction of the maxima of minor lobes in (6) can be approximated by letting $\sin\left(\frac{N}{2}\psi\right) = \pm 1$ in (9) when N is sufficiently large, which yields

$$\frac{N}{2}(kd\sin\theta - \beta)\,|_{\theta=\theta_s} = \pm\frac{2s+1}{2}\pi, \quad s = 0, 1, 2, \cdots, \tag{11}$$

$$\theta_{s1} = \arcsin\left\{\frac{\lambda}{2\pi d}\left[\beta \pm \frac{3\pi}{N}\right]\right\}. \tag{12}$$

From (11), when $s = 0$, θ_{s0} is in the direction of mainlobe, when $s = 1$, θ_{s1} in (12) is the maximum direction of first minor lobes, when $s = 2$, θ_{s2} is the maximum direction of second minor lobes, and so forth.

B. CATEGORIES OF WIDEBAND PHASE SHIFTERS
Wideband phase shifters can be roughly classified into four types [47], [56]: true phase shifters (TPSs), TTDs, true time delays with group delays and other types. For convenience, it also refers to TPS as ideal phase shifter and TTD as ideal time delay in this article.
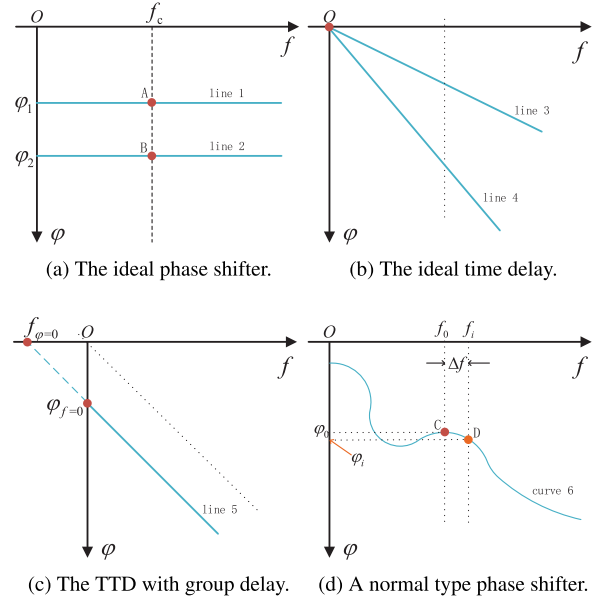

(a) The ideal phase shifter.   (b) The ideal time delay.

(c) The TTD with group delay.   (d) A normal type phase shifter.

FIGURE 2. Phase-frequency transfer function of a phase shifter.

1) IDEAL PHASE SHIFTER
In a narrowband system, the phase shifter always works at a specific center frequency. In Fig. 2a, points A and B are the states of a narrowband phase shifter working at center frequency f_c. In a wideband system, also as in Fig. 2a, lines 1 and 2 are two states of an ideal phase shifter, and in each state, the ideal wideband phase shifter maintains the same phase value over the operating frequency range.

2) IDEAL TIME DELAY
The TTD implies that the phase shifter maintains the same time delay over the operating frequency range. In (2), the phase φ is linearly related to the frequency f when the time delay τ is fixed, and the two states of the ideal time delay are represented by lines 3 and 4 through the origin in Fig. 2b, respectively.

3) IDEAL TIME DELAY WITH GROUP DELAY
As shown in Fig. 2c, the group phase delay of this phase shifter is $\phi_{f=0}$. The TTD can also be considered as a time delay without group delay.

4) OTHER TYPES OF NON-IDEAL PHASE SHIFTERS
Fig. 2d depicts a hypothetical other type of phase shifter. To the authors' knowledge, the design of such a phase shifter does not yet exist. However it is interesting when the function $\varphi(f)$ is controllable. Although this hypothetical phase shifter is given here, we will not explore any usage of it in this article.

C. MAIN BEAM DIRECTION
A phase shifter in the narrowband antenna array can be represented as $\varphi = 2\pi f_c \tau$, where f_c is the center frequency and τ is the time delay of the phase shifter. This relationship

can also be written as $\beta = 2\pi f_c \tilde{\tau}$, where β is the progressive phase difference of the phase shifter array as mentioned in Section II.A and $\tilde{\tau}$ is the corresponding progressive time delay difference.

For wideband arrays, the phase may vary with frequency, there is

$$\beta_i = 2\pi f_i \tilde{\tau}_i, \qquad (13)$$

and substituting (13) into (8) yields

$$\theta_m\,(f_i) = \arcsin \frac{c\tilde{\tau}_i}{d}. \qquad (14)$$

Formulas for the main beam direction in this subsection are summarized in Table 1.

TABLE 1. The main beam direction of the array with phase shifters in Section II.B.

Types of phase shifter	main beam direction θ_m
ideal time delay	$\arcsin \frac{c\tilde{\tau}}{d}$
ideal phase shifter	$\arcsin \frac{c\beta}{2\pi df_i}$
TTD with group delay	$\arcsin \left\{ \sin\theta_0 \left[\frac{f_0}{f_0 - f_{\varphi=0}} \cdot \left(1 - \frac{f_{\varphi=0}}{f_i}\right) \right] \right\}$
other kinds	$\arcsin \left[\sin\theta_0 \left(1 + \frac{f_{\varphi=0}}{f_0 - f_{\varphi=0}} \cdot \frac{\Delta f}{f_0 + \Delta f}\right) \right]$

1) ANTENNA ARRAYS USING IDEAL TIME DELAYS

For an array with ideal time delays, where the phase shifter has the same delay τ at any operating frequency and the array has a frequency-independent time delay difference $\tilde{\tau}$, there is

$$\theta_m\,(f_i) = \arcsin \frac{c\tilde{\tau}}{d}. \qquad (15)$$

In this case, the main beam direction of an array is completely independent of frequency. Alternatively, this phenomenon can be explained by Fig. 1, which is described in Section II.G.

2) ANTENNA ARRAYS USING IDEAL PHASE SHIFTERS

For beam steering arrays with equal array element spacing, if ideal phase shifters are used, there is a constant progressive phase difference of β at any operating frequency. By fixing β in (13) and substituting it into (14), we get

$$\theta_m\,(f_i) = \arcsin \frac{c\beta}{2\pi df_i}. \qquad (16)$$

3) ANTENNA ARRAYS USING IDEAL TIME DELAYS WITH GROUP DELAY

From Fig. 2c, the value of a phase shifter in the form of the ideal time delay with group delay at frequency f_i is

$$\varphi_i = -\frac{\varphi_{f=0}}{f_{\varphi=0}}\left(f_i - f_{\varphi=0}\right). \qquad (17)$$

From (17), we get

$$\beta_i = -\frac{\beta_{f=0}}{f_{\varphi=0}}\left(f_i - f_{\varphi=0}\right), \qquad (18)$$

where β is the corresponding progressive phase difference of the array, also recognized as the line passing through the

point $(f_{\varphi=0},0)$ in Fig. 2c and $\beta_{\varphi=0}$ is its value at the assumed frequency 0.

Precisely, we can obtain the relationship between φ_i and f_i from the two points on line 5 in Fig. 2c. Substituting (18) and (13) into (14), we get

$$\theta_m\,(f_i) = \arcsin \left[-\frac{c\beta_{f=0}}{2\pi df_{\varphi=0}} \left(1 - \frac{f_{\varphi=0}}{f_i}\right) \right]. \qquad (19)$$

When line 5 in Fig. 2c is used to represent a progressive phase difference β, for a point on it (f_0, β_0), θ_0 is the main beam direction at frequency f_0. Substituting $\frac{\beta_{f=0}}{-f_{\varphi=0}} = \frac{\beta_0}{f_0 - f_{\varphi=0}}$ and (8) into (19), we arrive at

$$\theta_m(f_i) = \arcsin \left\{ \sin\theta_0 \left[\frac{f_0}{f_0 - f_{\varphi=0}} \cdot \left(1 - \frac{f_{\varphi=0}}{f_i}\right) \right] \right\}. \qquad (20)$$

4) ANTENNA ARRAYS USING OTHER TYPES OF PHASE SHIFTERS

Fig. 2d describes the transfer function for a normal kind of phase shifter. In the first-order Taylor approximation, the relationship between phase and frequency near a certain frequency [47] is

$$\theta_m\,(f_i)|_{f_i=f_0+\Delta f} \approx \arcsin \left[\sin\theta_0 \left(1 + \frac{f_{\varphi=0}}{f_0 - f_{\varphi=0}} \cdot \frac{\Delta f}{f_0 + \Delta f}\right) \right], \qquad (21)$$

where (f_0, φ_0) is any point on the curve in Fig. 2d, Δf is the small frequency offset, θ_0 is the beam direction at frequency f_0, and $f_{\varphi=0}$ is the frequency of the tangent to the point (f_0, φ_0) on the curve when $\varphi = 0$. The derivation of (21) is omitted due to space limitations in this article.

D. BEAMWIDTH OF THE MAIN BEAM

Substituting (13) into (10) we get the 3 dB direction of the main beam, where

$$\theta_{\pm h}\,(f_i) \approx \arcsin \left(\frac{c}{d}\tilde{\tau}_i \pm \frac{2.782c}{2\pi dNf_i} \right). \qquad (22)$$

In (22), there are two parts in the arcsin function, the first part representing the beam direction of the main beam and the other part representing the 3 dB direction of the main beam. Broadly speaking, the range $[-\frac{2.782c}{2\pi dNf_i}, \frac{2.782c}{2\pi dNf_i}]$ in the second part represents the half-power range of the main beam, while in the first part, if the progressive time delay difference $\tilde{\tau}$ is larger, the main beam angle θ_m is larger.

Leveraging Fig. 3, we can shed light on the relationship of beam direction and beamwidth in (22). In Fig. 3 the x-axis describes the beam direction, whereas the y-axis represents the beam domain. x_1 and x_2 are the main beam direction of the two beams and are represented in the beam domain by y_1 and y_2, respectively. Δx_1 and Δx_2 are their HPBWs in the angular domain. Similarly, the HPBWs in the beam domain are Δy_1 and Δy_2, respectively. x_A and x_B are the 3 dB directions of the second beam. The curve in Fig. 3 is similar to the actual shape of the function $y = \sin x$ and does not affect the conclusions of the following analysis.
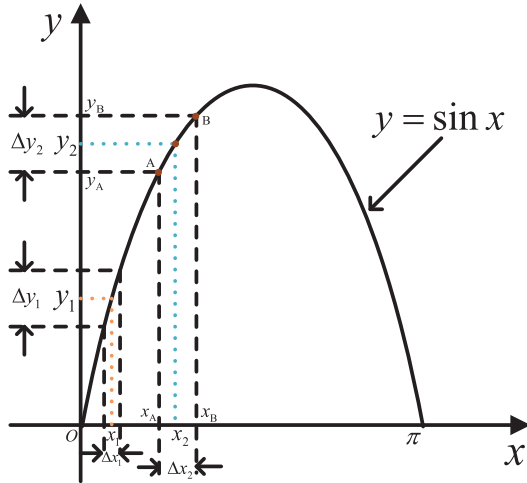
FIGURE 3. The relationship of beam direction and beamwidth in (22) by the function $y = \sin x$.

For the function $y = \sin x$, $x \in [0, \pi/2]$, (x_1, y_1), (x_2, y_2) are the points on the function, y_1 and y_2 are the center points on the interval Δy_1 and Δy_2, respectively, and if the value $\Delta y_1 = \Delta y_2$ and $x_1 < x_2$, then $\Delta x_1 < \Delta x_2$. In addition, $\Delta x_1 < \Delta x_2$ holds if $x_1 < x_2$ and $\Delta y_1 < \Delta y_2$. When $|y_2 - y_A| = |y_B - y_2|$, we have $|x_2 - x_A| < |x_B - x_2|$. This means that the 3 dB direction $|\theta_m(f_i) - \theta_{+h}(f_i)| < |\theta_m(f_i) - \theta_{-h}(f_i)|$. So, when θ is larger, more precisely, the HPBW can be written as

$$\Theta_h = |\theta_{-h} - \theta_{+h}|. \qquad (23)$$

From (22), the following conclusions can be drawn for wideband arrays:

- The broadside beam has the same beam orientation at all operating frequencies, $\theta_m(f_i) = 0$ as in Fig. 1, regardless of the phase shifter used in the array. Also, the broadside beam has a minimum HPBW at all frequencies, the higher the frequency, the smaller the beamwidth.
- For a particular frequency f_i, the beamwidth of the angular domain increases as the beam direction θ_m rises.
- With the same direction of the main beam, the larger the frequency, the smaller the beamwidth.
- In the beam domain, the beamwidth is independent of the beam direction and is inversely proportional to the number of antennas N, the spacing between antennas d and the operating frequency.
- For an array with ideal time delays, all frequencies have the same main beam direction θ_m.
- The main beam direction θ_m and the beamwidth in the beam domain decrease with increasing frequency for arrays with ideal phase shifters, as shown in (10).

In addition, the HPBW remains unchanged when the value of dNf_i is held constant with the same main beam orientation. This property may be useful in the array design.

E. FIRST SIDE LOBE DIRECTION

Comparing (12) with (10), the structures are similar, so the conclusions for 3 dB direction also hold for first sidelobe

direction as well.

$$\theta_{s1}(f_i) = \arcsin\left(\frac{c\tilde{\tau}_i}{d} \pm \frac{3c}{2dNf_i}\right). \qquad (24)$$

F. DIRECTION OF THE GRATING LOBE

Grating lobes occurs when (7) has other solutions, except when $m = 0$. Furthermore, the beam direction of the grating lobe is

$$\theta_g(f_i) = \arcsin\left(\frac{c\tilde{\tau}_i}{d} \pm \frac{\lambda_i}{d}m\right), \quad m = 1, 2, \cdots. \qquad (25)$$

Comparing (25) with (10), their structures are very similar. Thus the conclusion of the grating lobe is similar to that of HPBW, except for the following properties:

- The beam direction of the grating lobe is independent of the antenna number N and is determined by the main beam direction θ_m and the ratio of antenna spacing to working wavelength.
- For antenna arrays with fixed element spacing, if there is a grating lobe, the angle between the grating lobe and the main beam decreases as the frequency increases. This property holds for both arrays with ideal phase shifters and arrays with ideal time delays.

G. THE GENERATION OF BEAM SQUINTING

TTDs allow an antenna array to maintain a consistent main beam direction at different frequencies. In the example of the received beam of the linear array in Fig. 1, the delay difference between the array elements does not change with frequencies when the incidence angles of the beams are the same. So by exploiting the transceiver equivalence, it is possible to generate a wideband beam for this array that maintains a consistent main beam direction between different frequencies through TTDs. On the other hand, beam squinting between different frequencies is unavoidable for any wideband array employing other types of phase shifters. There are two main strategies to deal with beam squinting: (1) force squint beams of different frequencies into the same main beam direction to increase the performance of the point-to-point communication, and (2) exploit the spatial degrees of freedom of beam squinting to form multi-beam for multi-user. While both approaches are interesting, we are currently intrigued by the second one. Consequently, we will attempt to exploit the squinting characteristics of the array with ideal phase shifters in the following sections.

III. MILLIMETER-WAVE MULTI-TIER WIDEBAND ANTENNA ARRAY DESIGN

For an antenna array, the phase distribution of each antenna controls the direction of the main beam, while the amplitude distribution governs the beamwidth of the main beam and the amplitude level of the sidelobes [54, Chap. 1.5.1, Chap. 16.7.2], [57]. For all antenna array structures in Fig. 4, N_t is the number of antennas, N_{RF} is the number of RF chains, and N_s is the number of independent signal streams. Fig. 4a depicts a simplified structure of a conventional narrowband
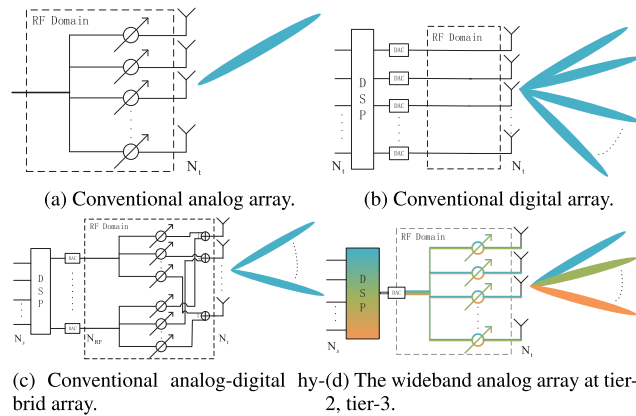
(a) Conventional analog array.

(b) Conventional digital array.

(c) Conventional analog-digital hybrid array.

(d) The wideband analog array at tier-2, tier-3.

FIGURE 4. The structure of several antenna arrays.

analog array, where the beam direction is controlled by a set of phase shifters connected to each antenna in the RF domain. If each antenna is equipped with a power amplifier, this array can further reduce the beamwidth of the main beam and the sidelobe amplitude. Without utilizing other methods, there is only one independent signal in the digital domain, and this array can only have one signal beam stream. In Fig. 4b, the digital array can simultaneously maintain the phase and amplitude of independent signal streams in the digital baseband domain. Since the array has a degree of freedom of N_t, it can add N_t independent elaborate beams to the digital domain, each of which can maintain an independent signal stream. For the hybrid analog-digital structure in Fig. 4c, multi-beam are implemented by adding sets of phase shifters to the antenna array in the RF domain. Interference among beams is reduced in the digital domain by adjusting the amplitude and phase of the group of signal streams carried for each RF chain. In general, as the number of independent signal streams is limited by the N_{RF}, this hybrid structure can maintain up to N_{RF} independent beams simultaneously. As the number of antennas in the array surges, especially in mmWave communication systems, hybrid precoding structures are attracting more and more attention. However, when it comes to very wideband scenarios, new problems are encountered and the design of the array structure needs to be reconsidered.

A. THE EFFECT OF WIDE BANDWIDTH ON ANTENNA ARRAY AND BEAMFORMING

1) THE EFFECT OF WIDE BANDWIDTH ON ANTENNA ELEMENT SPACING

Due to the abundance of frequency resources in the mmWave band, with wavelengths spanning nearly 10 times (in the frequency range of about 30∼300 GHz), there is a rather intuitive challenge in the design of wideband beamforming arrays with such large bandwidths, namely, the mismatch between the extremely wide working frequency range and the fixed distance of the antenna elements. The traditional narrowband structure with half-wavelength spacing between

elements implies that the design of antenna arrays serving very wide frequency bands should be reconsidered.

2) THE EFFECT OF WIDEBAND PHASE SHIFTERS ON BEAMFORMING

From (16), it is known that wideband arrays using ideal phase shifters encounter the problem of squinting of the main beam direction. Taking OFDM-based wideband hybrid structures as an example, the work in [28]–[30] assumes the use of separate digital precoders for each sub-carrier in the digital domain and a unified analog precoder in the RF domain. Thus, it forms a hybrid digital-analog precoding structure for each sub-carrier, while multiple sub-carrier in the analog domain share same RF chains and phase shifters. However, uniform wideband phase shifters imply the use of ideal phase shifters. In this case, each sub-band has its own main beam direction and its own HPBW, and a user may receive sub-carrier beams at different power levels or even only a portion of these beams. Thus, in mmWave ultra-wideband scenarios, antenna arrays using ideal phase shifters suffer from the beam squinting phenomenon.

3) THE EFFECT OF WIDE BANDWIDTH ON COST AND PERFORMANCE

From a cost savings perspective, wideband phase shifters and wideband RF chains are more expensive than the corresponding narrowband elements. So for a fully connected wideband hybrid structure, each RF chain is connected with a wideband phase shifter for each antenna, which may be overpriced and redundant for many wideband scenarios.

A solution may exist that takes advantage of the multi-band and compact nature of the fractal antenna array and the squinting multi-beam of the wideband array to serve multi-user. By dividing the antenna array into multi-tier through the concept of fractals, the array as a whole can operate over a very large wideband frequency range. Each of these tiers, as shown in Fig. 4d, has a wideband analog array operating in a relatively small wideband frequency range, which is structurally similar to a conventional analog beamforming array as shown in Fig. 4a. Although only one wideband phase shifter is connected to each antenna, and the array requires only one wideband RF chain, this structure can produce multi-beam with beam squinting, which is somewhat similar to the multi-beam capability of hybrid arrays. However, it is different from the traditional array structures used for communications today, and a number of technical details and shortcomings need to be addressed in the design and application.

B. THE mmWave WIDEBAND ANTENNA ARRAY DESIGN

Traditional wideband antennas, such as log-periodic antennas, cannot electrically change the direction of the beam and are too large to be used as elements for antenna arrays. There is an old Chinese proverb: "A hurricane starts with the slightest shaking of clover leaves, an awesome wave arises from wavelets." Combining the interesting self-similarity
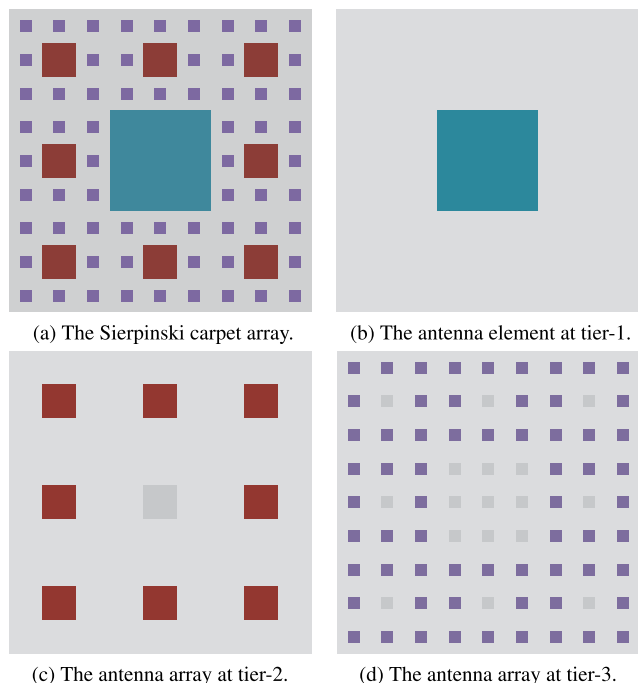
(a) The Sierpinski carpet array.

(b) The antenna element at tier-1.

(c) The antenna array at tier-2.

(d) The antenna array at tier-3.

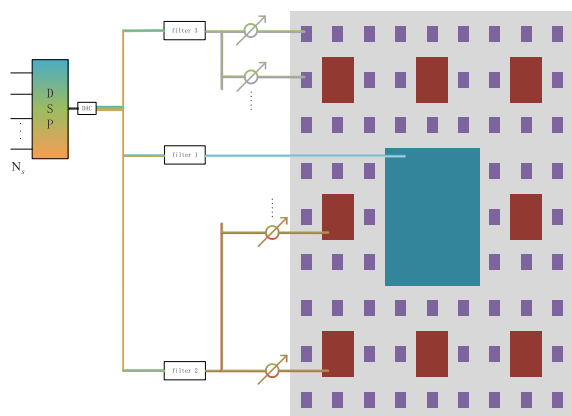**FIGURE 5.** A Sierpinski carpet antenna array with three antenna tiers.

FIGURE 6. The multi-wideband structure with the Sierpinski carpet array of three tiers.

properties of fractals with the powerful beams produced by a large number of low-gain antenna elements may be worth trying. We exploit the concept of the Sierpinski carpet fractal [22], [58] to form a multi-tier wideband antenna array structure, with each tier supporting a different wideband frequency region. Although this antenna array can have many tiers, we use only the first three tiers as in Fig. 5 (also the right half of Fig. 6) and the first four tiers as in Fig. 7a as an alternative. For arrays with more than four tiers, the patch antenna elements in the array may not be feasible and work beyond the mmWave band. While the gain per patch element is small, higher gains can be obtained with a large-scale microstrip patch antenna array.

1) ULTRA WIDEBAND ANTENNA ARRAY
The Sierpinski carpet antenna array is a compact, multi-band, and wideband planar array. For the Sierpinski carpet fractal
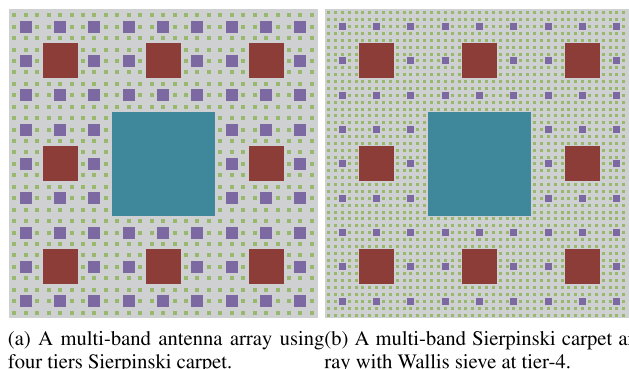

(a) A multi-band antenna array using four tiers Sierpinski carpet.

(b) A multi-band Sierpinski carpet array with Wallis sieve at tier-4.

FIGURE 7. Extentions and variations of the 3-tiers Sierpinski carpet array.

as in Fig. 5a, one-ninth of the tier area are cut off from the carpet in each tier, we regard the cut-off parts of the carpet as patch antennas and the grey lattice elements in Fig. 5c and Fig. 5d indicate missing elements in the rectangular planar arrays of tier-2 and tier-3. With half-wavelength spacing of the center frequency, the scale of center frequency between two neighboring tiers is threefold. In addition, the square patch elements in the Sierpinski carpet array have an edge length of one-sixth of the wavelength, which we assume to be reasonable even though their size is smaller than the usual edge lengths between one-third and half-wavelength [54, Chap.14]. On the other hand, the Dielectric Resonator Antenna (DRA) [59]–[61] could be used as element in the array for its smaller size, larger antenna gain, and relatively wider bandwidth compared with the Microstrip Patch Antenna (MPA).

The transceiver structure in Fig. 6 is a Sierpinski carpet antenna array using three tiers of wideband analog arrays. The center frequency of the array is determined by the spacing of the elements in each tier. In this structure, a wideband RF chain is connected to each antenna element separately via a wideband phase shifter. In addition, since each antenna element belongs to a specific array tier and each wideband phase shifter has its own determined operating frequency range, then although three tiers share a wideband RF chain, each tier can operate independently in a different frequency range through filter 1, 2, and 3 of tier-1, tier-2, and tier-3, respectively.

As stated above, the spacing scale of the elements between two adjacent tiers of the Sierpinski carpet antenna array is tripled. When the array operates in narrowband mode, each tier uses a precise half-wavelength antenna spacing, assuming that the first three tiers operate at frequencies f_1, f_2, and f_3, where $f_2 = 3f_1$ and $f_3 = 3f_2$, respectively. In the wideband mode, when the operating frequency range of each tier is assumed to be $[\frac{1}{2}f_1, \frac{3}{2}f_1]$, $[\frac{1}{2}f_2, \frac{3}{2}f_2]$ and $[\frac{1}{2}f_3, \frac{3}{2}f_3]$. Therefore, the entire array can cover the frequency range of $[\frac{1}{2}f_1, \frac{3}{2}f_3]$. In each tier, the ratio of the antenna spacing to the operating wavelength is at $[\frac{1}{4}, \frac{3}{4}]$. It is too idealized to make this assumption: first, the total transmit power in the system is limited and we can work well in part of the frequency range; second, a quarter wavelength antenna spacing of the array is

not efficient for a communication system; third, when the antenna spacing is between one-half and one wavelength, although there is only one grating lobe, the probability of grating lobe increases as the antenna spacing increases. So the final result is that the operating wavelength should not deviate too much from twice the antenna spacing.

2) THE FIRST TIER FOR LOW RATE COMMUNICATION

As in Fig. 5b, the first tier has only one antenna and no array gain to compensate for the high attenuation. So we can place here an antenna that operates at frequencies below 5 GHz, with a center frequency that is not one-third that of tier-2. In this case, the array length depends on the frequency of tier-2. Because the lower frequency band has less air attenuation and good scattering performance, but a relatively narrow bandwidth, this tier is suitable for low-rate data communications and information feedback for users. It should be noted that the first tier has only one antenna connected to the RF chain, so there is no need for an analog phase shifter. If there are multiple Sierpinski carpet arrays forming a large array, this tier forms the digital baseband array structure of Fig. 4b.

### 3) THE WIDEBAND ANALOG STRUCTURE IN TIER-2 AND TIER-3

Tier-2 and tier-3 can each form a wideband analog array operating in different frequency bands. In the tier-2 array shown in Fig. 5c, there are eight antenna elements, each of which is connected to the wideband RF chain with a separate wideband phase shifter. By employing ideal phase shifters to give the wideband array the beam squinting characteristic, multi-beam can thus be formed simultaneously. As shown in Fig. 5d, tier-3 has a total of 64 antenna elements, which is eight times the number of antennas in tier-2. Because there are more antenna elements at this tier, it is reasonable to use lower radiated power and less expensive antenna elements at tier-3 to obtain similar array gain as tier-2. The wideband analog structure in Fig. 4d is substantially different from the narrowband analog beamforming structure in Fig. 4a. First, in Fig. 4d RF chains and phase shifters are wideband components. Second, in the digital baseband domain, it is more complicated to combine multiple signal streams into a single RF chain, whereas in Fig. 4a there is only one signal stream. Finally, the wideband analog structure can form multiple squint beams, while the narrowband analog structure can only form an individual beam.

4) EXTENTIONS AND VARIATIONS OF THE THREE TIERS SIERPINSKI CARPET ARRAY

If a fourth tier is needed, both a four tiers Sierpinski carpet array as in Fig. 7a and a Wallis sieve in tier-4 ($f_4 = 5f_3$) as in Fig. 7b are feasible.

C. THE SIERPINSKI CARPET ARRAYS OF DIFFERENT SIZES AND THEIR POSSIBLE APPLICATION SCENARIOS

Fig. 8 shows the atmospheric absorption properties of the electromagnetic waves. In the frequency range of mmWave,
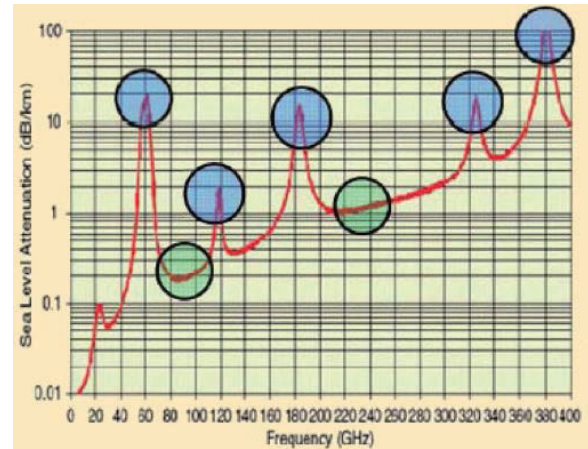
FIGURE 8. The properties of atmospheric absorption of electromagnetic waves. (Figure from Fig. 1 of [62] and also from Fig. 2 of [63].)

there are about three mountaintops with high atmospheric attenuation, 60, 120, and 180 GHz, and not far from mmWave are 22 GHz and 322 GHz. The attenuation at 60, 180, and 322 GHz is comparable to about 20 dB/Km, and at 120 GHz is about 2 dB/Km. In addition, the attenuation at 45 GHz is about 0.2 dB/Km.

There are also large atmospheric windows suitable for long-range communications [63]: (1) the attenuation in the window range from 210 to 300 GHz is close to the line from 1 to 2 dB/Km, (2) the attenuation in the window range from about 73 to 110 GHz is close to the line from 0.2 to 0.3 dB/Km, and (3) the attenuation in the window range from about 124 to 160 GHz can be approximated to the line from 0.4 to 0.6 dB/Km. Although the attenuation of about 1 to 2 dB/Km is high, the large frequency bandwidth of 210 to 300 GHz is also very attractive.

1) THE 20, 60, AND 180 GHz ARRAY FOR SHORT-RANGE SECURE COMMUNICATION

When the element spacing is half wavelength of the center frequency, the side length of the square array is 7.5 mm because the wavelength of the first tier at 20 GHz is 15 mm. At 60 GHz, the element spacing of tier-2 is 2.5 mm, and the spacing of the tier-3 at 180 GHz is about 0.833 mm.

2) THE 30, 90, AND 270 GHz ARRAY

The array utilizes two large air windows, a window around 90 GHz and a window around 240 GHz. In addition, arrays with center frequencies of 28, 84, and 252 GHz are more appropriate.

3) THE 5, 15, 45, AND 135 GHz ARRAY

With the four tiers Sierpinski carpet fractal structure shown in Fig. 7a, it is possible to design a square array of 5, 15, 45, and 135 GHz with side lengths of 3 cm.

4) THE 5, 15, 45, AND 225 GHz ARRAY

As shown in Fig. 7b, the array at tier-4 can operate at 225 GHz using the Wallis sieve concept, and because of the large

atmospheric window in this band, this array may be suitable for short-range communications that require large bandwidths.

D. mmWave MULTI-SUBARRAY DESIGN

The Sierpinski square structure in Fig. 6 is suitable for forming larger antenna arrays. Fig. 9a shows a large array with four Sierpinski subarrays. In the first tier, there is a digital baseband array structure, so sophisticated digital beamforming techniques can be used in this tier. Fig. 9b shows a similar structure for tier-2 and tier-3, although the center frequency and operating frequency range are different for these two tiers. This large array can operate in either subarray mode or large array mode. In the subarray mode, each subarray can perform beam steering independently. Whereas, in large array mode, phase compensation in the digital domain is used to save the cost of the phase shifters in each subarray, as will be explained in Section V.
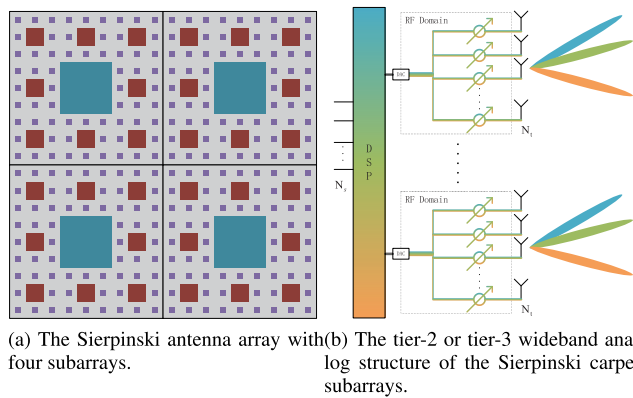

FIGURE 10. Simplified design of phase shifters by cell selection in the array.

(a) The Sierpinski antenna array with four subarrays.

(b) The tier-2 or tier-3 wideband analog structure of the Sierpinski carpet subarrays.

FIGURE 9. Sierpinski Antenna array with four subarrays.

IV. HOW MANY CELLS ARE NEEDED IN A PLANAR ARRAY?

When a wideband phase shifter is implemented by cascading wideband cells [47], and each cell has the same ideal phase-shifting frequency-phase characteristics as in Fig. 2a, we can obtain a uniformly quantized ideal phase shifter. Further, in order to reduce the cost and simplify the design, all the phase shifters in the array can be implemented by selecting cells from the cascade of cells as shown in Fig. 10. Arrays with this design can still enable steering beams, and the important parameters of the wideband array design become the design of the frequency-phase characteristics of the cells and the selection of the total number of cells in the array. In addition, since the number of cells required for this design is not affected by the missing elements in the array, the number of cells required for tier-2 and tier-3 in Fig. 5 can also be derived using the planar array with no missing array elements in this section.

For a planar array placed on the x-y plane, as in Fig. 11, there are M antenna elements placed along the x-axis with spacing and progressive phase shifts of d_x and β_x, respectively. And similarly, the number of antenna elements placed
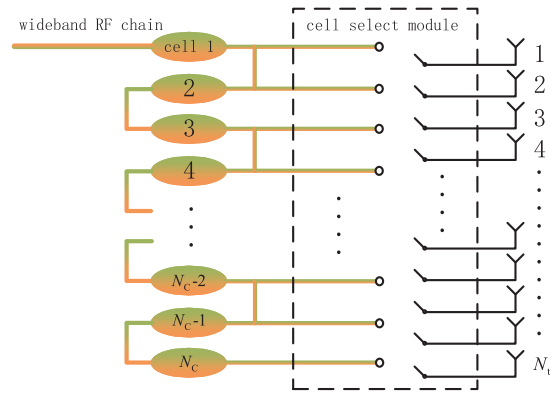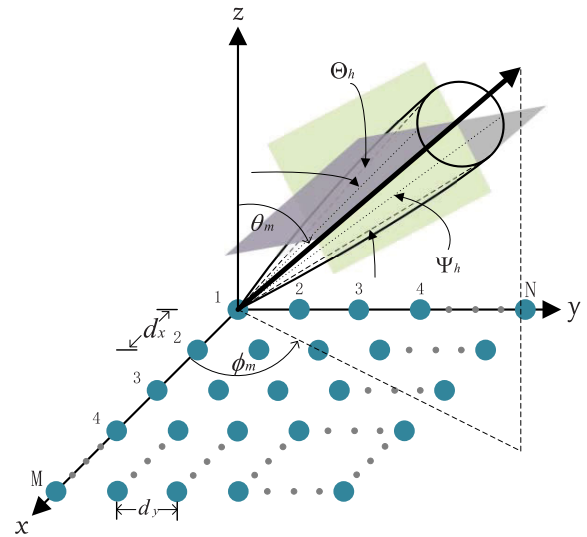

FIGURE 11. Planar array geometries, main beam directions, and HPBWs.(Combined with Fig. 6.30b and Fig. 6.38 in [54].)

along the y-axis, their spacing, and the progressive phase shift between the elements are denoted by N, d_y, and β_y, respectively. The main beam is steering along $\theta = \theta_m$ and $\phi = \phi_m$, and HPBWs in the vertical plane of the main beam and in its tangent plane along the direction of the main beam are denoted by Θ_h and Ψ_h, respectively.

Rewrite (6-93a) and (6-93b) in [54] to obtain

$$\beta_x = kd_x \sin \theta_m \cos \phi_m, \tag{26}$$

$$\beta_y = kd_y \sin \theta_m \sin \phi_m, \tag{27}$$

where the wavenumber k is related to the working frequency.

From (26) and (27) we have

$$\phi_m = \arctan\left(\frac{\beta_y d_x}{\beta_x d_y}\right), \tag{28}$$

$$\theta_m = \arcsin\left(\frac{c}{2\pi f_i}\sqrt{\left(\frac{\beta_x}{d_x}\right)^2 + \left(\frac{\beta_y}{d_y}\right)^2}\right). \tag{29}$$

From (28), the angle ϕ_m of the main beam direction is determined by the element spacing and the progressive

phase shift, which means that when these parameters are fixed to the array, ϕ_m will remain constant and will not vary with frequency. Thus the beam squinting method that matches well with linear arrays does not cover all angles for planar arrays in 3-D scenarios. (With ideal phase shifters, the trace of squint beams is a perpendicular line in the $\phi_m - \theta_m$ plane, and with other kinds of phase shifters it is a curve in the $\phi_m - \theta_m$ plane.) Therefore, additional work is needed to refine the beam squinting approach on planar arrays.

As mentioned above in this section, in order to save the cost of the phase shifters, the phase shifters in the array share a number of cascaded phase shift cells, as shown in Fig. 10. The values of progressive phase shifts can also be written as $\beta_x = m\beta_{cell}$ and $\beta_y = n\beta_{cell}$, where β_{cell} is the phase shift of one cell in the array. When $d_x = d_y = d$, (28) and (29) can be reduced to

$$\phi_m = \arctan \frac{n}{m}, \tag{30}$$

$$\theta_m = \arcsin \left(\frac{c\beta_{cell}}{2\pi d f_i} \sqrt{m^2 + n^2} \right). \tag{31}$$

From (30) and (31) we have

$$m = \frac{2\pi d f_i \sin \theta_m \cos \phi_m}{c\beta_{cell}}, \tag{32}$$

$$n = \frac{2\pi d f_i \sin \theta_m \sin \phi_m}{c\beta_{cell}}, \tag{33}$$

which means that when the beam direction is fixed, the higher the frequency, the greater the value of m and n. In addition, with half-wavelength spacing, m and n drop to $\pi \sin \theta_m \cos \phi_m / \beta_{cell}$ and $\pi \sin \theta_m \sin \phi_m / \beta_{cell}$. Also, since the progressive phase shift is composed of an integer number of phase cells, we get $\widetilde{m} \in \{\lfloor m \rfloor, \lceil m \rceil\}$ and $\widetilde{n} \in \{\lfloor n \rfloor, \lceil n \rceil\}$.

The HPBWs Φ_h and Θ_h can be approximated by (6-98) and (6-99) in [54] as

$$\Theta_h = 1 \bigg/ \sqrt{\cos^2 \theta_m \left[\Theta_{x0}^{-2} \cos^2 \phi_m + \Theta_{y0}^{-2} \sin^2 \phi_m \right]}, \tag{34}$$

$$\Psi_h = 1 \bigg/ \sqrt{\Theta_{x0}^{-2} \sin^2 \phi_m + \Theta_{y0}^{-2} \cos^2 \phi_m}, \tag{35}$$

where Θ_{x0} and Θ_{y0} are the HPBWs of the linear array placed on the x- and y-axis, respectively, when the beam direction is along the z-axis. It is consistent with the HPBW when $\theta = 0$ in Fig. 1, so we can obtain Θ_{x0} from (23) and (22) by setting the time delay $\tau_i = 0$, namely

$$\Theta_{x0}(f_i) \approx 2 \arcsin \left(\frac{2.782c}{2\pi d M f_i} \right). \tag{36}$$

Similarly, we can obtain Θ_{y0} by replacing M in (36) with N. Moreover, when $M = N$ we get $\Theta_{x0} = \Theta_{y0}$, then (34) and (35) simplify to $\Theta_h = \Theta_{x0} / \cos \theta_m$ and $\Psi_h = \Theta_{x0}$, respectively.

When designing an antenna array, the maximum phase shifts of the phase shifters in the array should be within the phase range represented by all cascading cells in the array,

that is, $(M-1)\beta_x + (N-1)\beta_y \leq N_c \beta_{cell}$, where N_c represents the maximum number of phase shift cells in the array, and by dividing by β_{cell} we get

$$(M-1)m + (N-1)n \leq N_c. \tag{37}$$

From the perspective of beam angular coverage, the main beam should cover all the angle range. When the array spacing is one-half of working wavelength, setting the maximum θ_m in (31) to θ_{max} yields

$$m^2 + n^2 = \left(\frac{\pi \sin \theta_{max}}{\beta_{cell}} \right)^2. \tag{38}$$

We can obtain the smallest N_c in the $m - n$ plane by the tangent point of the circle denoted by (38) and a cluster of lines denoted by (37). When $M = N$, from (38) we get $m = n = \left\lfloor \pi \sin \theta_{max} / \sqrt{2} \beta_{cell} \right\rfloor$, then from (37) we get $N_c = 2(M - 1)m$.

TABLE 2. Cell Number N_c for the Sierpinski carpet array.

N_c	Tier-2	Tier-3	Tier-4
$\beta_{cell} = 0.01, \phi_{max} = 90°$	888	3552	11544
$\beta_{cell} = 0.01, \phi_{max} = 60°$	768	3072	9984
$\beta_{cell} = 0.1, \phi_{max} = 90°$	88	352	1144
$\beta_{cell} = 0.1, \phi_{max} = 60°$	76	304	988
$\beta_{cell} = 0.5, \phi_{max} = 90°$	16	64	208
$\beta_{cell} = 0.5, \phi_{max} = 60°$	12	48	156

Table 2 shows the maximum cell number needed in each tier of the Sierpinski carpet array calculated from (37) and (38). When $\theta_{max} = 90°$, $M = N = 3$, $\beta_{cell} = 0.01$, $N_c = 888$; when $\theta_{max} = 90°$, $M = N = 9$, $\beta_{cell} = 0.01$, $N_c = 3552$. Moreover, it is inefficient to set $\theta_{max} = 90°$ in a practical system and for a wideband array we can get a beam with a larger θ_{max} by squinting to lower frequencies. When $\theta_{max} = 60°$, $M = N = 3$, $\beta_{cell} = 0.01$, $N_c = 768$; when $\theta_{max} = 60°$, $M = N = 9$, $\beta_{cell} = 0.01$, $N_c = 3072$. With the examples above, N_c decreases significantly when setting θ_{max} from 90° to 60°, which is linear with $\sin \theta_{max}$.

From the perspective of cost-saving, in this section, we use a group of cells to substitute the phase shifters in the array. In addition, the cell number in an array could be decreased by limiting the maximum perpendicular angle of the main beam. Furthermore, by compensating in digital domain, it is feasible to form large arrays for beam steering without increasing the number of cells per subarray. The disadvantages of this design are that the assumption of the cascaded cell-based phase-shifting network is well idealized without considering the way of feeding in the RF design and that we only leverage the beam steering without considering the more complicated beam pattern synthesis methods for the FRPS.

V. BEAM STEERING AND BEAM ADAPTING ALGORITHM

We consider the downlink beamforming of a system with a BS and N users.[2] The BS is equipped with four subarrays as shown in Fig. 9a and one subarray for each user. Each subarray has three tiers, as in Fig. 5. The first tier is used for channel information feedback, and the second tier and the third tier are used for data streams transmission to the users.

For each subarray of the BS, it is possible to work for a primary user at tier-2 and tier-3, respectively. These two tiers may also operate for a single primary user only, by using two scattering paths to increase the overall rate or reduce the probability of communication outages of the user. Besides, all subarrays of the BS can also operate uniformly in the large array mode, which can provide higher array gain compared to the subarray mode. This mode can be used in the channel estimation stage where channel conditions are uncertain, or to further improve the transmission performance for users with poor channel conditions. In addition, when the beams of the primary users at tier-2 and tier-3 are determined, there may be one or more scattering paths suitable for the secondary users, in which case the required operating frequencies of the beams in the direction of scattering paths can be calculated and the array response vector of the primary user can be multiplexed by the beam squinting method.

The first stage is the channel estimation or path angle-of-departure (AoD) and angle-of-arrival (AoA) estimation stage, which is assumed to be completed. Then there is the data transmission stage using beam steering, where beam adaptive algorithms are used to establish or maintain the link. A significant difference between this process and previous work is that the operating frequency of the secondary user will change as the beam direction varies.

A. CHANNEL MODEL

For a planar antenna array with M rows and N columns as in Fig. 11, the array response of a steering beam with the main beam direction of (ϕ_m, θ_m) can be represented as

$$
\begin{aligned}
\mathbf{A}(\phi_m,\theta_m) &= \mathbf{A}(\beta_x, \beta_y) \\
&= \mathbf{a}(\beta_x, M)\mathbf{a}(\beta_y, N)^T \\
&= \mathbf{a}(\beta_x, M) \otimes \mathbf{a}(\beta_y, N)^T \\
&\overset{(a)}{=} \frac{1}{\sqrt{MN}}
\begin{bmatrix}
e^{-j\varphi_{11}} & \cdots & e^{-j\varphi_{1N}} \\
\vdots & \ddots & \vdots \\
e^{-j\varphi_{M1}} & \cdots & e^{-j\varphi_{MN}}
\end{bmatrix} \\
&= \frac{\begin{bmatrix}
1 & \cdots & e^{-j(N-1)\beta_y} \\
\vdots & \ddots & \vdots \\
e^{-j(M-1)\beta_x} & \cdots & e^{-j((M-1)\beta_x+(N-1)\beta_y)}
\end{bmatrix}}{\sqrt{MN}}, \quad (39)
\end{aligned}
$$

[2]For simplicity, formula derivations, algorithms, and simulations in this and the next section are based on the ideal rectangular planar array, since the Sierpinski carpet tier can be interpreted as an antenna array with either missing elements or elements failure, which mainly increases the main beamwidth and sidelobe level of the steering beam [64]–[68], and does not affect the feasibility of the beam squinting algorithms in this section. For more accurate results, the AF in Appendix A can be exploited in this section.

where $\mathbf{a}(\beta_x, M)$ is the beam steering array response of a linear array with M antenna elements and β_x progressive phase shift along the x-axis, $\mathbf{a}(\beta_y, N)^T$ is the beam steering array response of a linear array with N antenna elements and a progressive phase shift of β_y along the y-axis. (a) hold for constant modulus of elements in the linear array response $\mathbf{a}$, such as when an analog antenna array is used. φ_{ij} is the value of the ideal phase shifter for the antenna placed in row i and column j of the array. The relationship between the progressive phase shift with main beam direction is elucidated by (26) and (27). The linear array response can be expressed in terms of $\mathbf{a}(\beta, M) = \frac{1}{\sqrt{M}}[1, e^{-j\beta}, \ldots, e^{-j(M-1)\beta}]^T$.

The array response in (39) could be rewritten into vector form as

$$
\begin{aligned}
\mathbf{a}(\phi_m, \theta_m) &= \mathbf{a}(\beta_x, \beta_y) \\
&= vec(\mathbf{A}(\phi_m, \theta_m)) \\
&= [e^{-j\varphi_{11}}, \ldots, e^{-j\varphi_{M1}}, \ldots, \\
&\quad \ldots, e^{-j\varphi_{1N}}, \ldots, e^{-j\varphi_{MN}}]^T / \sqrt{MN}. \quad (40)
\end{aligned}
$$

For arrays with omnidirectional radiated antenna elements, the radiation amplitude beam pattern can be approximated by AF. Therefore, the steering beam power pattern of a planar array with progressive phase shift β_x and β_y along x- and y-axis can be represented as $B(\phi, \theta) = |AF(\phi, \theta)|^2$, where

$$
\begin{aligned}
AF(\phi, \theta) &\overset{(b)}{=} AF(\psi_x) AF(\psi_y) \\
&= \mathbf{a}(\phi, \theta)^H \mathbf{a}(\phi_m, \theta_m) \\
&= \mathbf{a}(\phi, \theta)^H \mathbf{a}(\beta_x, \beta_y) \\
&= \sum_{i=1}^{M} \sum_{j=1}^{N} \{\mathbf{A}(\phi, \theta)^* * \mathbf{A}(\beta_x, \beta_y)\}_{ij}, \quad (41)
\end{aligned}
$$

(b) from (6-88) in [54], where $AF(\psi)$ is the AF of a linear array, as expressed by (6). ψ_x and ψ_y are the total progressive phase difference for the beam along the direction of x- and y-axis, respectively. And similar to (5), we have

$$
\psi_x = kd_x \sin\theta \cos\phi - \beta_x, \quad (42)
$$
$$
\psi_y = kd_y \sin\theta \sin\phi - \beta_y. \quad (43)
$$

Extending to mmWave scenario [13] with the Saleh-Valenzuela model [69], there are N_c scatterers, and the ith scatterer has a cluster with N_{pi} paths. It should be emphasized that each scatterer may have a different number of paths, which is different from the channel model in [13]. The possible channel model for an antenna array working at frequency f is

$$
\mathbf{H} = \sum_{c=1}^{N_c} \sum_{l=1}^{N_{pc}} \alpha_{cl} \mathbf{a}_r(\phi_{cl}^r, \theta_{cl}^r) \mathbf{a}_t(\phi_{cl}^t, \theta_{cl}^t)^H. \quad (44)
$$

In this article, it is assumed that the BS maintains only one beam path with each user, so it is reasonable to assume that each scatterer contributes one possible beam path under this condition. Thus the possible channel model for any user in

(44) can be rewritten as

$$\mathbf{H}_i(f) = \sum_{l=1}^{N_{ci}} \alpha_l(f) \mathbf{a}_r(\phi_l^r, \theta_l^r) \mathbf{a}_t(\phi_l^t, \theta_l^t)^H, \tag{45}$$

$$\mathbf{H}_i(f) = \sum_{l=1}^{N_{ci}} \alpha_l(f) \mathbf{a}_r\left(\beta_{xl}^r(f), \beta_{yl}^r(f)\right) \mathbf{a}_t\left(\beta_{xl}^t(f), \beta_{yl}^t(f)\right)^H. \tag{46}$$

In fact only one beam path is selected in (45). Also implicit in (45) is the main beam direction in relation to the operating frequency for an array response of an antenna array employing ideal phase shifters, as shown by (46). $\alpha_l(f)$ is the complex gain of the lth beam, which is related to the reflection and absorption conditions of the scatterer, as well as to the absorption of the path in the air. Since it is assumed that a scatterer has only one path, the coefficient of any path should not be too small. In addition, when the BS is operating in subarray mode, the size of the array response vector $\mathbf{a}_t$ in (45) is only dependent on the size of the subarray. For small subarray sizes and long path beams, the angular difference resulting from selecting a different subarray can be neglected.

B. BEAM STEERING

We derive in Appendix B the conditions for point-to-point communication using two non-line-of-sight (NLoS) beams at either tier-2 or tier-3, however it is very demanding for the location of the scatterers. But the conditions are somewhat relaxed when the planar array shown in Fig. 11 uses squint beams to communicate with two users. The favored two users only need to have scatterers with similar ϕ values in the direction-of-departure (DoD). Therefore, in this subsection, we use tier-2 or tier-3 on the BS side to serve multi-user as an enhancement of these tiers, without adding an RF chain.

For analog precoding matrices in traditional hybrid structures, as in Fig. 4c, the number of rows represents the number of antennas and the number of columns is the group of phase shifters connected to the antenna array. In fact, the position relationship of antenna elements in a planar array can also be represented by a matrix, which is often rewritten in vector form as an array response vector for convenience.

The BS uses four Sierpinski carpet subarrays to form a larger square array, as shown in Fig. 9a. $\mathbf{X}$ is a matrix of transmitted signals from the planar array at the BS side, which can be denoted as

$$\begin{aligned}
\mathbf{X} &= \begin{bmatrix} \mathbf{F}_{11} & \mathbf{F}_{12} \\ \mathbf{F}_{21} & \mathbf{F}_{22} \end{bmatrix} \odot \left(\begin{bmatrix} e^{-j\varphi_{11}^B} & e^{-j\varphi_{12}^B} \\ e^{-j\varphi_{21}^B} & e^{-j\varphi_{22}^B} \end{bmatrix} * \begin{bmatrix} s_{11} & s_{12} \\ s_{21} & s_{22} \end{bmatrix} \right) \\
&= \begin{bmatrix} \mathbf{F}_{11}e^{-j\varphi_{11}^B} & \mathbf{F}_{12}e^{-j\varphi_{12}^B} \\ \mathbf{F}_{21}e^{-j\varphi_{21}^B} & \mathbf{F}_{22}e^{-j\varphi_{22}^B} \end{bmatrix} \odot \begin{bmatrix} s_{11} & s_{12} \\ s_{21} & s_{22} \end{bmatrix} \\
&= \begin{bmatrix} \mathbf{X}_{11} & \mathbf{X}_{12} \\ \mathbf{X}_{21} & \mathbf{X}_{22} \end{bmatrix},
\end{aligned} \tag{47}$$

where $\mathbf{X}_{mn}$ represents the matrix of the transmitted signals for the mth row and n^{th} column subarray of the larger array,

and can be written as

$$\mathbf{X}_{mn} = \mathbf{F}_{mn}e^{-j\varphi_{mn}^B}s_{mn}, \quad m, n = 1, 2, \tag{48}$$

$$\mathbf{F} = \begin{bmatrix} \mathbf{F}_{11}e^{-j\varphi_{11}^B} & \mathbf{F}_{12}e^{-j\varphi_{12}^B} \\ \mathbf{F}_{21}e^{-j\varphi_{21}^B} & \mathbf{F}_{22}e^{-j\varphi_{22}^B} \end{bmatrix}. \tag{49}$$

1) BEAM STEERING IN LARGE ARRAY MODE

In this article, it is assumed that the phase shifter is composed of cascading cells, in which case the number of cells in the phase shifter should be increased to achieve a higher phase shift or time delay. Thus, when a beam in the same main direction is realized through a large array, the phase shifter of some of the antennas requires more cells than a small array. In order to save the number of cells in the subarray and to simplify the precoding in the analog domain, in the large array mode, all subarrays have the same analog precoding matrix, which is $\mathbf{F}_{11} = \mathbf{F}_{12} = \mathbf{F}_{21} = \mathbf{F}_{22}$, and the phase or delay difference between the subarrays is handled in the digital domain. When a subarray is used as a reference subarray there is $\varphi_{11} = 0$ and the phase or delay differences of the other subarrays with respect to it are $\varphi_{21} = M\beta_x$, $\varphi_{12} = M\beta_y$ and $\varphi_{22} = \varphi_{21} + \varphi_{12} = M(\beta_x + \beta_y)$. Moreover, in the large array mode, the input signals of different subarrays should be the same, that is, $s_{11} = s_{12} = s_{21} = s_{22}$.

The processed signal received by the user i at tier-2 or tier-3 at frequency f can be written as

$$\begin{aligned}
y_i &= vec(\mathbf{W}_i)^H \, r_i(f) \\
&\overset{(c)}{\approx} vec(\mathbf{W}_i)^H \left\{ \sqrt{\rho}\mathbf{H}_i(f) vec(\mathbf{X}(f)) + n_i(f) \right\} \\
&= \sqrt{\rho} vec(\mathbf{W}_i)^H \mathbf{H}_i(f) \, vec\left(\begin{bmatrix} e^{-j\varphi_{11}^B} & e^{-j\varphi_{12}^B} \\ e^{-j\varphi_{21}^B} & e^{-j\varphi_{22}^B} \end{bmatrix} \otimes \mathbf{F}_{11} \right) s_i \\
&\quad + vec(\mathbf{W}_i)^H n_i(f) \\
&\overset{(d)}{=} \sqrt{\rho}\mathbf{w}_i^H \mathbf{H}_i(f) \mathbf{f} \, s_i + \mathbf{w}_i^H n_i(f) \\
&\overset{(e)}{\approx} \sqrt{\rho}\alpha_l(f) \left\{ vec(\mathbf{w}_i)^H \mathbf{a}_r(\phi_l^r, \theta_l^r) \right\} \left\{ \mathbf{a}_t(\phi_l^t, \theta_l^t)^H \mathbf{f} s_i \right\} \\
&\quad + \mathbf{w}_i^H n_i(f),
\end{aligned} \tag{50}$$

where r_i is the received signal at frequency f. (c) assumes that the mmWave channel is noise limited, where the interference power of steering beams from other users is dissipated in the air and is ignored. (d) is achieved by rewriting $\mathbf{w} = vec(\mathbf{W})$ and $\mathbf{f} = vec(\mathbf{F}) = vec\left(\begin{bmatrix} e^{-j\varphi_{11}^B} & e^{-j\varphi_{12}^B} \\ e^{-j\varphi_{21}^B} & e^{-j\varphi_{22}^B} \end{bmatrix} \otimes \mathbf{F}_{11} \right)$, where $\mathbf{F}$ is a simulated precoding matrix of the large array simulated by subarrays with a much smaller number of phase-shifting cells, each of which is cascaded with a complex value in the digital domain to maintain the steering precoding of the large array. (e) is based on the assumption that the actual channel has one scatterer and that this scatterer has only one path for simplicity. ρ is the average received power level.

The net result of (e) is to seek an optimal path among the possible channels, and then to generate the steering beam corresponding to this path by precoding and combining matrices in order to obtain the maximum spectral efficiency. Then the

spectral efficiency of user i is

$$R_i = log_2\left(1 + \frac{\rho\alpha_l^2(f)}{\sigma_n^2 \mathbf{w}_i^H \mathbf{w}_i} \mathbf{w}_i^H \mathbf{a}_r(\phi_l^r, \theta_l^r)\mathbf{a}_t(\phi_l^t, \theta_l^t)^H \mathbf{f}\right.$$

$$\times \mathbf{f}^H \mathbf{a}_t(\phi_l^t, \theta_l^t)\mathbf{a}_r(\phi_l^r, \theta_l^r)^H \mathbf{w}_i\left.\right)$$

$$\overset{(f)}{=} log_2\left(1 + \frac{\rho\alpha_l^2(f)|\mathbf{w}_i^H \mathbf{a}_r(\phi_l^r, \theta_l^r)\mathbf{a}_t(\phi_l^t, \theta_l^t)^H \mathbf{f}|^2}{\sigma_n^2}\right), \quad (51)$$

where (f) is obtained by noting that there is $\mathbf{w}_i^H \mathbf{w}_i = 1$ when utilizing the steering combing matrix $\mathbf{w}_i$ of (40), and that the conjugate transpose of a complex value is its conjugate.

In subarray mode, each subarray at the BS operates independently with a single wideband RF chain, respectively. Besides, the derivation of the beam steering rate in subarray mode is omitted since it is not used in the simulation.

C. ADAPTION ALGORITHMS WITH BEAM SQUINTING

Algorithm 1 gives the steps for system initialization or beam adaption as the primary user moves. The primary user operates at frequency f_c, which corresponds to twice the wavelength of the spacing in the array. The reason for calculating the virtual AoA operating at f_c in steps 6 and 7 is that the number of cells used cannot exceed the design maximum number of cells in the subarray. From (32) and (33), it is clear that if frequencies beyond f_c are used directly, the number of cells required may exceed the designed maximum number of cells for the subarray.

Algorithm 2 shows the beam adapting steps when the secondary user moves, where the main body of Algorithm 2 could be recognized as steps 4 to 7 in Algorithm 1. Comparing Algorithms 1 with 2, it is more complicated when the primary user moves for the reason that the secondary users share the phase shifters of the primary user at the BS. Thus, when the beam of the primary user is updated, all the secondary users should adapt their working frequencies to the new array response vector.

In the next section, we only use Algorithm 1 to simulate the initialization stage of the system, while omitting the movement of the primary or secondary users.

VI. SIMULATION RESULTS

In this section, we present simulation results to demonstrate the feasibility of combining the arrays presented in Section III with the algorithms presented in Section V to serve multi-user. We consider the case where there is only one BS and multi-user, where the BS has four subarrays as shown in Fig. 9a and one subarray per user as shown in Fig. 6. As described in Section V, the first tier is used for channel information feedback and tier-2 and tier-3 are used to transmit the data streams of the users. To illustrate the use of this array and to reduce the design complexity, the BS only works in the large array mode consisting of four subarrays, as shown in Fig. 9, although larger arrays with more subarrays are acceptable, and each subarray can also work separately.

Algorithm 1 System Initialization Or Beam Adaption When the Primary User Is Moving

---

Input: The BS gets the new AoD $(\theta_{new}^t, \phi_{new}^t)$ for the moved primary user and AoD (θ_s^t, ϕ_s^t) for the secondary user. The primary user updates the new AoA $(\theta_{new}^r, \phi_{new}^r)$. The AoA for the secondary user is (θ_s^r, ϕ_s^r).

1: The BS updates the transmitting phase shifters by the new AoD $(\theta_{new}^t, \phi_{new}^t)$ of the primary user according to (32) and (33):

$$\widetilde{m}_t = \left\lfloor \frac{2\pi d f_c \sin\theta_{new}^t \cos\phi_{new}^t}{c\beta_{cell}} \right\rfloor,$$
$$\widetilde{n}_t = \left\lfloor \frac{2\pi d f_c \sin\theta_{new}^t \sin\phi_{new}^t}{c\beta_{cell}} \right\rfloor.$$

2: The primary user updates the transmitting phase shifters by the new AoA $(\theta_{new}^r, \phi_{new}^r)$ according to (32) and (33):

$$\widetilde{m}_r = \left\lfloor \frac{2\pi d f_c \sin\theta_{new}^r \cos\phi_{new}^r}{c\beta_{cell}} \right\rfloor,$$
$$\widetilde{n}_r = \left\lfloor \frac{2\pi d f_c \sin\theta_{new}^r \sin\phi_{new}^r}{c\beta_{cell}} \right\rfloor.$$

3: **if** $\phi_s^t \in [\phi_{new}^t - \Psi_h/2, \phi_{new}^t + \Psi_h/2]$ **then**

4:     Update the frequency of the squint beam for this secondary user based on (31): $f_s = \frac{c\beta_{cell}}{2\pi d \sin\theta_s^t}\sqrt{\widetilde{m}_t^2 + \widetilde{n}_t^2}$.

5:     Feedback f_s to this secondary user with the first tier.

6:     This secondary user computes the virtual AoA (θ_c^r, ϕ_c^r) of the virtual squint beam working at f_c based on (31), where $\theta_c^r = \arcsin(f_s \sin\theta_s^r/f_c)$ and $\phi_c^r = \phi_s^r$.

7:     This secondary user updates the receiving phase shifters by f_s and the AoA (θ_c^r, ϕ_c^r) according to (32) and (33):

$$\widetilde{m}_s = \left\lfloor \frac{2\pi d f_c \sin\theta_c^r \cos\phi_c^r}{c\beta_{cell}} \right\rfloor,$$
$$\widetilde{n}_s = \left\lfloor \frac{2\pi d f_c \sin\theta_c^r \sin\phi_c^r}{c\beta_{cell}} \right\rfloor.$$

8: **else**

9:     The BS terminates or rejects the enhanced beam service for this secondary user, reports and provides feedback.

10: **end if**

11: **for all** other secondary users in the request enhanced beam list **do**

12:     Update the AoD (θ_s^t, ϕ_s^t) and AoA (θ_s^r, ϕ_s^r) for this secondary user.

13:     **goto** step 3.

14: **end for**

We leverage the extended Saleh-Valenzuela model for modeling users' channels [13]. Each user works at a particular frequency, and its channel contains several uniformly distributed clusters, each consisting of multi-path whose angles conform to a Laplacian distribution, where each path can be represented by the array response vector at that frequency with the path's AoA, AoD angle information, and a path gain coefficient. For a path in each cluster, its AoA and AoD angles obey a Laplacian distribution with standard variance corresponding to the spread of angles in that cluster, respectively. For the channel of any user, satisfying $\mathbb{E}[\| \mathbf{H} \|_F^2] = N_t N_r$, the complex gain coefficient α_{il} for the lth ray in the ith cluster

---

Algorithm 2 Beam Adaption When a Secondary User Moves

Input: The BS gets the new AoD $(\theta^t_{new}, \phi^t_{new})$ for the moved user and the $\widetilde{m}_t, \widetilde{n}_t$ of the transmitting array. The secondary user updates the new AoA $(\theta^r_{new}, \phi^r_{new})$.

1: **if** $\phi^t_{new} \in [\phi^t_{old} - \Psi_h/2, \phi^t_{old} + \Psi_h/2]$ **and** $\theta^t_{new} \notin [\theta^t_{old} - \Theta_h/2, \theta^t_{old} + \Theta_h/2]$ **then**

2:     Update the frequency of the squint beam based on (31):
$$f_{new} = \frac{c\beta_{cell}}{2\pi d \sin\theta_m}\sqrt{\widetilde{m}_t^2 + \widetilde{n}_t^2}.$$

3:     Feedback f_{new} to the user with the first tier.

4:     This secondary user computes the virtual AoA (θ^r_c, ϕ^r_c) of the virtual squint beam working at f_c based on (31), where $\theta^r_c = \arcsin(f_{new}\sin\theta^r_{new}/f_c)$ and $\phi^r_c = \phi^r_{new}$.

5:     This user updates the receiving phase shifters by f_s and the AoA (θ^r_c, ϕ^r_c) according to (32) and (33):
$$\widetilde{m}_s = \left\lfloor \frac{2\pi d f_c \sin\theta^r_c \cos\phi^r_c}{c\beta_{cell}} \right\rfloor,$$
$$\widetilde{n}_s = \left\lfloor \frac{2\pi d f_c \sin\theta^r_c \sin\phi^r_c}{c\beta_{cell}} \right\rfloor.$$

6: **else if** $\phi^t_{new} \notin [\phi^t_{old} - \Psi_h/2, \phi^t_{old} + \Psi_h/2]$ **then**

7:     The BS terminates the enhanced beam service for this secondary user, reports and provides feedback.

8: **end if**

---

follows the i.i.d. complex Gaussian distribution $\mathcal{CN}(0, \sigma^2_{\alpha,i})$, where $\sigma^2_{\alpha,i} = \frac{N_t N_r}{N_{cl} N_{ray}}$ is the average power of the path in the cluster. However, this constraint on channel power is broken by the processing of removing paths outside the range of the allowed sectors, and more details on this can be found in [13].

In the simulation of [13], each user has $N_{cl} = 8$ clusters, and each cluster has $N_{ray} = 10$ paths. We find that even if the strongest path is removed from the channel, the original optimal steering beam may have a considerable rate in many cases, due to the fact that small cluster angle spread such as 7.5° and large HPBW angles result in a strong correlation between the array response vectors of the two rays in the cluster. To circumvent this problem, the number of rays can be set to $N_{ray} = 1$. In addition, in some cases a smaller number of clusters may be more appropriate.

In this simulation, the center working frequency of the tier-1, tier-2, and tier-3 are 15, 45, and 135 GHz respectively. To reflect the differences in the scattering environment experienced by each user, the random number of clusters N_{cl} for each user channel is set from 1 to 8, and the random number of paths N_{ray} is set from 1 to 10, but still keeping the angle spread of the clusters to 7.5°. The average channel power for users at the same tier is the same. For convenience, each user shares the same path in tier-2 and tier-3, and the different path attenuation due to atmospheric absorption between these two tiers is ignored. Unlike [13], the arrays in this article are all placed in the x-y plane, and both the elevation angle θ and azimuthal ϕ of the main beam are in the range of [0°, 90°]. Because only a positive number of cells can be selected through (32) and (33), the arrays cannot directly support a large angular range, but the [0°, 360°] range of ϕ can also be achieved by selecting the reference antenna element. The sectors are set to

[0°, 90°] in both azimuth and elevation angles. It is important to note that antenna arrays of BS and users can have their own independent coordinate system.

The maximum number of achievable steering beams is determined by the power constraint of the BS and is not limited in the simulation. The signal-to-noise ratio (SNR) is defined as $\frac{\rho}{\sigma^2_n}$, where we set the received SNR to 0 dB and assume that the signals and noises follow the i.i.d. $\mathcal{CN}(0, 1)$. To simplify the design, the HPBW in step 3 of Algorithm 1 is set to a constant value of $\Psi_h = \Theta_{x0}(f_c)$ according to (36), where f_c is the center frequency of that tier. Finally, all results are reported for averaged over 10000 random channel realizations. Unless otherwise mentioned, these parameters are used for the experiments.
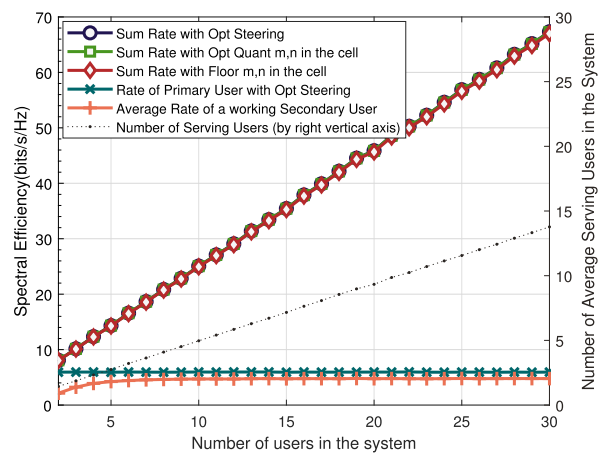
FIGURE 12. Tier-2, $\beta_{cell} = 0.1$.

Fig. 12 shows the spectral efficiency achieved by tier-2 when $\beta_{cell} = 0.1$. The number of serving users in tier-2 increases almost linearly with the number of randomly placed users in the system. The non-integer value of the number of service users is due to averaging over multiple trials. By simply flooring the number of cells in steps 1 and 2 of Algorithm 1, the sum rate of the steering beams in the system is even close to the sum rate of the optimal steering beams. Although the array response vector of the BS is carefully prepared for the steering beam of the only primary user in the system, some of the secondary users can also use this array response vector to obtain comparatively low rates through squint beams. In Fig. 13, the performance of Algorithm 1 using the simple downward integer operation degrades when $\beta_{cell} = 0.5$. A more complex rounding method can be used to select the beam closest to the optimal steering beam, and the sum rate is still quite close to the optimal sum rate.

Fig. 14 and 15 show the spectral efficiency achieved by tier-3. When $\beta_{cell} = 0.1$, the quantization beam has sufficient quantization accuracy, so that the sum rate remains high even when only floor quantization is taken. However, when $\beta_{cell} = 0.5$, the performance of the sum rate decreases drastically with simple downward integer quantization, and
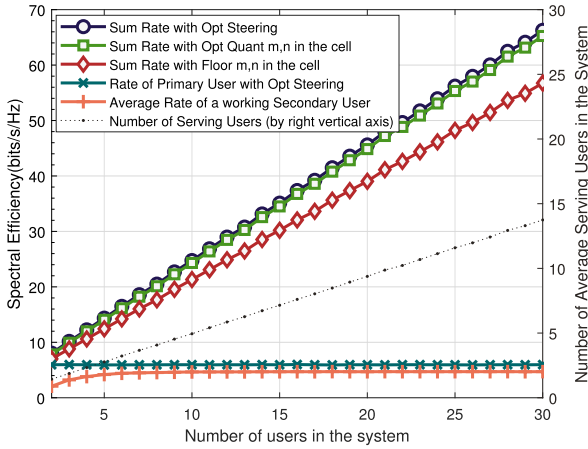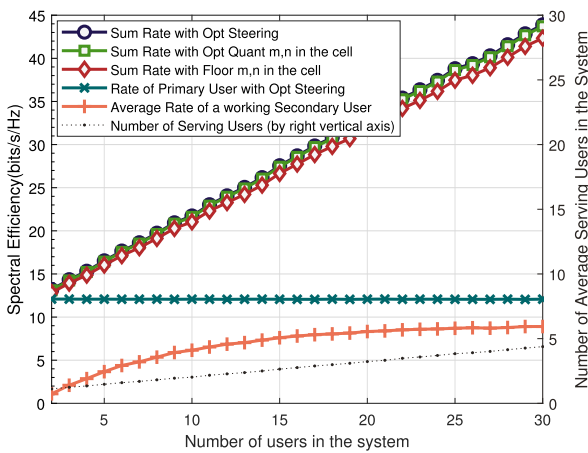
FIGURE 13. Tier-2, $\beta_{cell} = 0.5$.

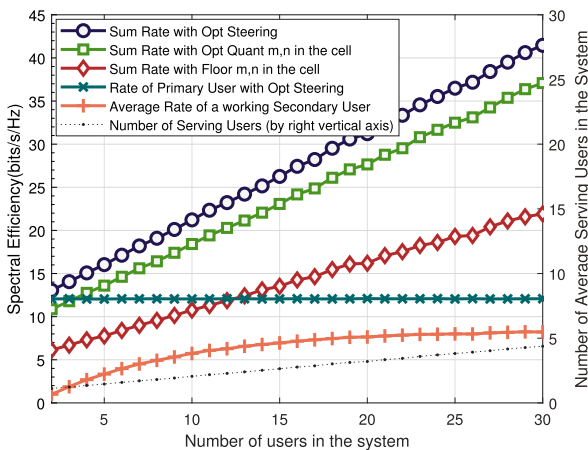**FIGURE 14.** Tier-3, $\beta_{cell} = 0.1$.

FIGURE 15. Tier-3, $\beta_{cell} = 0.5$.

the system still has a large sum rate when the optimal quantization value is used.

Comparing Fig. 12 and 14, the number of users served in tier-3 is less than in tier-2 due to the selection of suitable secondary users within the HPBW in step 3 of Algorithm 1.

From (35) and (36), it can be seen that Ψ_h decreases as the number of antennas increases, thus the probability of suitable secondary users in tier-3 decreases. We note that the optimal steering beam rate for the primary user in tier-3 is significantly higher than in tier-2. This is due to the fact that the average channel power in tier-3 is larger than in tier-2, as known by $\mathbb{E}[\| \mathbf{H} \|_F^2] = N_t N_r$, because tier-3 has more antenna elements. In tier-3, however, the average rate of the activated secondary users does not increase significantly, because the beams in tier-3 have better directivity, which in turn increases the directional error of the squint beams.

In summary, when the value of β_{cell} is sufficiently small, e.g., 0.1, floor quantization in Algorithm 1 is more appropriate, simple, and has minimal rate loss at both tier-2 and tier-3. When β_{cell} is not small enough, resulting in insufficient quantized beam resolution, it is then necessary to choose the optimal quant m and n values to recover the sum rate loss.

VII. CONCLUSION

In this article, we considered the design of mmWave multi-user communication schemes that exploit compact multi-wideband antenna arrays and squinting multi-beam characteristics. First, we derived the beam properties of the wideband array. Then, using the concept of fractals we designed a coplanar array that can work over three frequency bands in the mmWave frequency range. Afterwards, we replaced the phase shifter in the array with a cell-based design. Finally, based on the beam squinting property of the wideband array with ideal phase shifters, we designed the squinting multi-beam algorithm that supports multi-user communications and demonstrated its performance through simulation. For future work, it would be interesting to consider the application of the proposed array structure to mmWave small cell dense networks, as it is possible to avoid the problem of restricted azimuth of the squint beam by selecting a suitable small BS. In addition, more realistic channel models that can represent the differences in scattering environments between tiers due to atmospheric absorption would need to be addressed. Also, both the non-isotropic pattern and the mutual coupling of the antenna elements would need further analysis when implementing the realistic wideband squinting array. And last but not least, more practical fractal array architectures suitable for mmWave and sub-mmWave communication scenarios would be of great interest.

APPENDIX A
ARRAY FACTOR FOR TIER-2 AND TIER-3

In [22], the Sierpinski carpet array is considered as a two-dimentional Cantor set with a generator of

$$\mathbf{G} = \begin{bmatrix} 1 & 1 & 1 \\ 1 & 0 & 1 \\ 1 & 1 & 1 \end{bmatrix}. \qquad (52)$$

In order to establish a connection with the ordinary rectangular antenna array, we define a set of mask matrices $\{\mathbf{M}_p\}$,

each of which is a Sierpinski carpet array, where

$$\mathbf{M}_p = \mathbf{M}_{p-1} \otimes \mathbf{G}, \quad p = 2, 3, \cdots. \quad (53)$$

By setting $\mathbf{M}_1 = 1$, we get

$$\mathbf{M}_2 = \begin{bmatrix} 1 & 1 & 1 \\ 1 & 0 & 1 \\ 1 & 1 & 1 \end{bmatrix}, \quad (54)$$

$$\mathbf{M}_3 = \begin{bmatrix} 1 & 1 & 1 & 1 & 1 & 1 & 1 & 1 & 1 \\ 1 & 0 & 1 & 1 & 0 & 1 & 1 & 0 & 1 \\ 1 & 1 & 1 & 1 & 1 & 1 & 1 & 1 & 1 \\ 1 & 1 & 1 & 0 & 0 & 0 & 1 & 1 & 1 \\ 1 & 0 & 1 & 0 & 0 & 0 & 1 & 0 & 1 \\ 1 & 1 & 1 & 0 & 0 & 0 & 1 & 1 & 1 \\ 1 & 1 & 1 & 1 & 1 & 1 & 1 & 1 & 1 \\ 1 & 0 & 1 & 1 & 0 & 1 & 1 & 0 & 1 \\ 1 & 1 & 1 & 1 & 1 & 1 & 1 & 1 & 1 \end{bmatrix}. \quad (55)$$

The zero elements in $\mathbf{M}_p$ can be considered to be missing or turned off antenna elements at the corresponding positions, so the grey antenna elements of tier-2 and tier-3 in Fig. 5c and Fig. 5d can be considered to be missing antenna elements, corresponding one-to-one with the zero elements at the corresponding positions in the mask matrix in (54) and (55), respectively.

Then, the array response[3] for a Sierpinski carpet tier could be written as

$$\widetilde{\mathbf{A}}_p(\phi_m, \theta_m) = \mathbf{A}_p(\phi_m, \theta_m) * \mathbf{M}_p, \quad p = 2, 3, \cdots, \quad (56)$$

where $\mathbf{A}_p$ is the array response in the matrix form in (39) and has the same dimension with $\mathbf{M}_p$.

Note that from the viewpoint of the array antennas, the array response of the Sierpinski carpet array tier in (56) is normalized by the total number of antennas containing the missing array elements, and appropriate adjustments need to be made if the number of array elements of the Sierpinski carpet array tier is used for normalization.

Afterwards, substituting (56) into (40) and (41) gives the AF of the Sierpinski carpet array tier.

APPENDIX B
PREREQUISITE FOR THE ENHANCED POINT-TO-POINT COMMUNICATION BY TWO SCATTERERS AT TIER-2 OR TIER-3

In point-to-point NLoS mmWave communications, both the transmitter and the receiver use a planar array, as in Fig. 11, and we attempt to exploit the two scatterers between them by means of the beam squinting approach.

Suppose there are two path, (ϕ_1^t, θ_1^t) and (ϕ_1^r, θ_1^r) are the AoD and AoA of the first path, and similarly, (ϕ_2^t, θ_2^t) and (ϕ_2^r, θ_2^r) are the AoD and AoA of the second path. $m_t \beta_{cell}$ and $n_t \beta_{cell}$ are the progressive phase shifts on x- and y-axis at the transmitting side. $m_r \beta_{cell}$ and $n_r \beta_{cell}$ are the corresponding progressive phase shifts at the receiving side.

---

[3] A similar approach is adopted in [70] to obtain the actual array response, which covers the other element failure cases in addition to the cases of partial elements totally failed or missing.

If there exist two squint beams pairs at frequencies f_1 and f_2 along these two paths respectively, it is known from (30) that they need to satisfy the necessary conditions $\phi_1^t = \phi_2^t$ and $\phi_1^r = \phi_2^r$, due to the fact that the two transmitting beams share the same transmitting array with wideband phase shifters, and this is also true for the receiving side.

Furthermore, from (31) we get

$$\sin \theta_1^t = \frac{c\beta_{cell}}{2\pi d f_1} \sqrt{m_t^2 + n_t^2}, \quad (57)$$

$$\sin \theta_1^r = \frac{c\beta_{cell}}{2\pi d f_1} \sqrt{m_r^2 + n_r^2}, \quad (58)$$

$$\sin \theta_2^t = \frac{c\beta_{cell}}{2\pi d f_2} \sqrt{m_t^2 + n_t^2}, \quad (59)$$

$$\sin \theta_2^r = \frac{c\beta_{cell}}{2\pi d f_2} \sqrt{m_r^2 + n_r^2}. \quad (60)$$

(57) divided by (59) is $\frac{\sin \theta_1^t}{\sin \theta_2^t} = \frac{f_2}{f_1}$, (58) divided by (60) is $\frac{\sin \theta_1^r}{\sin \theta_2^r} = \frac{f_2}{f_1}$. As a consequence, the prerequisite for this enhanced communication is

$$\frac{\sin \theta_1^t}{\sin \theta_2^t} = \frac{\sin \theta_1^r}{\sin \theta_2^r}. \quad (61)$$

Only when (61) holds can we choose the appropriate frequencies f_1 and f_2 for the two paths. In fact, this is a harsh scattering condition when using square antenna arrays. In addition, if a line-of-sight (LoS) path exists, the user can maintain both a LoS path and a NLoS path at the same time. Since the LoS path has well signal strength, the receiver does not need a corresponding beam for reception, and therefore both sides can transmit squint beams for this LoS path at their respective required frequencies.
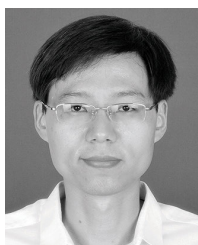
REFERENCES

[1] Z. Pi and F. Khan, "An introduction to millimeter-wave mobile broadband systems," *IEEE Commun. Mag.*, vol. 49, no. 6, pp. 101–107, Jun. 2011.

[2] J. G. Andrews, S. Buzzi, W. Choi, S. V. Hanly, A. Lozano, A. C. K. Soong, and J. C. Zhang, "What will 5G be?" *IEEE J. Sel. Areas Commun.*, vol. 32, no. 6, pp. 1065–1082, Jun. 2014.

[3] R. W. Heath, N. González-Prelcic, S. Rangan, W. Roh, and A. M. Sayeed, "An overview of signal processing techniques for millimeter wave MIMO systems," *IEEE J. Sel. Topics Signal Process.*, vol. 10, no. 3, pp. 436–453, Apr. 2016.

[4] A. S. Y. Poon and M. Taghivand, "Supporting and enabling circuits for antenna arrays in wireless communications," *Proc. IEEE*, vol. 100, no. 7, pp. 2207–2218, Jul. 2012.

[5] S. Kutty and D. Sen, "Beamforming for millimeter wave communications: An inclusive survey," *IEEE Commun. Surveys Tuts.*, vol. 18, no. 2, pp. 949–973, 2nd Quart., 2016.

[6] D. Gesbert, M. Shafi, D.-S. Shiu, P. J. Smith, and A. Naguib, "From theory to practice: An overview of MIMO space-time coded wireless systems," *IEEE J. Sel. Areas Commun.*, vol. 21, no. 3, pp. 281–302, Apr. 2003.

[7] T. L. Marzetta, "Noncooperative cellular wireless with unlimited numbers of base station antennas," *IEEE Trans. Wireless Commun.*, vol. 9, no. 11, pp. 3590–3600, Nov. 2010.

[8] F. Rusek, D. Persson, B. K. Lau, E. G. Larsson, T. L. Marzetta, and F. Tufvesson, "Scaling up MIMO: Opportunities and challenges with very large arrays," *IEEE Signal Process. Mag.*, vol. 30, no. 1, pp. 40–60, Jan. 2013.

[9] S. Bellofiore, C. A. Balanis, J. Foutz, and A. S. Spanias, "Smart-antenna systems for mobile communication networks. Part 1. Overview and antenna design," *IEEE Antennas Propag. Mag.*, vol. 44, no. 3, pp. 145–154, Jun. 2002.

[10] W. Hong, Z. H. Jiang, C. Yu, J. Zhou, P. Chen, Z. Yu, H. Zhang, B. Yang, X. Pang, M. Jiang, Y. Cheng, M. K. T. Al-Nuaimi, Y. Zhang, J. Chen, and S. He, "Multibeam antenna technologies for 5G wireless communications," *IEEE Trans. Antennas Propag.*, vol. 65, no. 12, pp. 6231–6249, Dec. 2017.

[11] Y. Aslan, J. Puskely, A. Roederer, and A. Yarovoy, "Active multiport subarrays for 5G communications," in *Proc. IEEE-APS Topical Conf. Antennas Propag. Wireless Commun. (APWC)*, Sep. 2019, pp. 298–303.

[12] X. Zhang, A. F. Molisch, and S.-Y. Kung, "Variable-phase-shift-based RF-baseband codesign for MIMO antenna selection," *IEEE Trans. Signal Process.*, vol. 53, no. 11, pp. 4091–4103, Nov. 2005.

[13] O. E. Ayach, S. Rajagopal, S. Abu-Surra, Z. Pi, and R. W. Heath, Jr., "Spatially sparse precoding in millimeter wave MIMO systems," *IEEE Trans. Wireless Commun.*, vol. 13, no. 3, pp. 1499–1513, Mar. 2014.

[14] T. J. Peters, "Phase-only synthesis for multiple beam phased arrays with element failures," in *IEEE Antennas Propag. Soc. Int. Symp. Dig.*, Jun. 1992, pp. 1352–1355.

[15] N. Garcia, H. Wymeersch, C. Fager, and E. G. Larsson, "mmWave hybrid array with more users than RF chains," 2017, *arXiv:1709.05200*. [Online]. Available: http://arxiv.org/abs/1709.05200

[16] N. Ishikawa, R. Rajashekar, S. Sugiura, and L. Hanzo, "Generalized-spatial-modulation-based reduced-RF-chain millimeter-wave communications," *IEEE Trans. Veh. Technol.*, vol. 66, no. 1, pp. 879–883, Jan. 2017.

[17] A. Morsali, A. Haghighat, and B. Champagne, "Realizing fully digital precoders in hybrid A/D architecture with minimum number of RF chains," *IEEE Commun. Lett.*, vol. 21, no. 10, pp. 2310–2313, Oct. 2017.

[18] L. He, J. Wang, and J. Song, "On generalized spatial modulation aided millimeter wave MIMO: Spectral efficiency analysis and hybrid precoder design," *IEEE Trans. Wireless Commun.*, vol. 16, no. 11, pp. 7658–7671, Nov. 2017.

[19] W. Wang and W. Zhang, "Transmit signal designs for spatial modulation with analog phase shifters," *IEEE Trans. Wireless Commun.*, vol. 17, no. 5, pp. 3059–3070, May 2018.

[20] E. Zhang and C. Huang, "On achieving optimal rate of digital precoder by RF-baseband codesign for MIMO systems," in *Proc. IEEE 80th Veh. Technol. Conf. (VTC-Fall)*, Sep. 2014, pp. 1–5.

[21] D. H. Werner and P. L. Werner, "Frequency-independent features of self-similar fractal antennas," *Radio Sci.*, vol. 31, no. 6, pp. 1331–1343, Nov. 1996.

[22] D. H. Werner, R. L. Haupt, and P. L. Werner, "Fractal antenna engineering: The theory and design of fractal antenna arrays," *IEEE Antennas Propag. Mag.*, vol. 41, no. 5, pp. 37–58, Oct. 1999.

[23] D. H. Wqrner and S. Ganguly, "An overview of fractal antenna engineering research," *IEEE Antennas Propag. Mag.*, vol. 45, no. 1, pp. 38–57, Feb. 2003.

[24] J. P. Gianvittorio and Y. Rahmat-Samii, "Fractal antennas: A novel antenna miniaturization technique, and applications," *IEEE Antennas Propag. Mag.*, vol. 44, no. 1, pp. 20–36, Aug. 2002.

[25] C. Puente-Baliarda, J. Romeu, R. Pous, and A. Cardama, "On the behavior of the sierpinski multiband fractal antenna," *IEEE Trans. Antennas Propag.*, vol. 46, no. 4, pp. 517–524, Apr. 1998.

[26] G. Walker and J. James, "Fractal volume antennas," *Electron. Lett.*, vol. 34, no. 16, pp. 1536–1537, 1998.

[27] H. Oraizi and S. Hedayati, "Miniaturized UWB monopole microstrip antenna design by the combination of giusepe peano and sierpinski carpet fractals," *IEEE Antennas Wireless Propag. Lett.*, vol. 10, pp. 67–70, 2011.

[28] A. Alkhateeb and R. W. Heath, "Frequency selective hybrid precoding for limited feedback millimeter wave systems," *IEEE Trans. Commun.*, vol. 64, no. 5, pp. 1801–1818, May 2016.

[29] F. Sohrabi and W. Yu, "Hybrid analog and digital beamforming for mmWave OFDM large-scale antenna arrays," *IEEE J. Sel. Areas Commun.*, vol. 35, no. 7, pp. 1432–1443, Jul. 2017.

[30] S. Park, A. Alkhateeb, and R. W. Heath, "Dynamic subarrays for hybrid precoding in wideband mmWave MIMO systems," *IEEE Trans. Wireless Commun.*, vol. 16, no. 5, pp. 2907–2920, May 2017.

[31] R. J. Mailloux, *Phased Array Antenna Handbook*. Norwood, MA, USA: Artech House, 2017.

[32] J. H. Brady and A. M. Sayeed, "Wideband communication with high-dimensional arrays: New results and transceiver architectures," in *Proc. IEEE Int. Conf. Commun. Workshop (ICCW)*, Jun. 2015, pp. 1042–1047.

[33] M. Cai, K. Gao, D. Nie, B. Hochwald, J. N. Laneman, H. Huang, and K. Liu, "Effect of wideband beam squint on codebook design in phased-array wireless systems," in *Proc. IEEE Global Commun. Conf. (GLOBE-COM)*, Dec. 2016, pp. 1–6.

[34] B. Liu, W. Tan, H. Hu, and H. Zhu, "Hybrid beamforming for mmWave MIMO-OFDM system with beam squint," in *Proc. IEEE 29th Annu. Int. Symp. Pers., Indoor Mobile Radio Commun. (PIMRC)*, Sep. 2018, pp. 1422–1426.

[35] J. P. Gonzalez-Coma, W. Utschick, and L. Castedo, "Hybrid LISA for wideband multiuser millimeter-wave communication systems under beam squint," *IEEE Trans. Wireless Commun.*, vol. 18, no. 2, pp. 1277–1288, Feb. 2019.

[36] B. Wang, M. Jian, F. Gao, G. Y. Li, and H. Lin, "Beam squint and channel estimation for wideband mmWave massive MIMO-OFDM systems," *IEEE Trans. Signal Process.*, vol. 67, no. 23, pp. 5893–5908, Dec. 2019.

[37] M. Wang, F. Gao, N. Shlezinger, M. F. Flanagan, and Y. C. Eldar, "A block sparsity based estimator for mmWave massive MIMO channels with beam squint," *IEEE Trans. Signal Process.*, vol. 68, pp. 49–64, 2020.

[38] H. Li, M. Li, Q. Liu, and A. L. Swindlehurst, "Dynamic hybrid beamforming with low-resolution PSs for wideband mmWave MIMO-OFDM systems," *IEEE J. Sel. Areas Commun.*, vol. 38, no. 9, pp. 2168–2181, Sep. 2020.

[39] Z. Sattar, J. V. C. Evangelista, G. Kaddoum, and N. Batani, "Antenna array gain and capacity improvements of ultra-wideband millimeter wave systems using a novel analog architecture design," *IEEE Wireless Commun. Lett.*, vol. 9, no. 3, pp. 289–293, Mar. 2020.

[40] Z. Wang, L. Cheng, J. Wang, and G. Yue, "Digital compensation wideband analog beamforming for millimeter-wave communication," in *Proc. IEEE 87th Veh. Technol. Conf. (VTC Spring)*, Jun. 2018, pp. 1–5.

[41] Z. Liu, W. ur Rehman, X. Xu, and X. Tao, "Minimize beam squint solutions for 60 GHz millimeter-wave communication system," in *Proc. IEEE 78th Veh. Technol. Conf. (VTC Fall)*, Sep. 2013, pp. 1–5.

[42] M. Longbrake, "True time-delay beamsteering for radar," in *Proc. IEEE Nat. Aerosp. Electron. Conf. (NAECON)*, Jul. 2012, pp. 246–249.

[43] T.-S. Chu and H. Hashemi, "True-time-delay-based multi-beam arrays," *IEEE Trans. Microw. Theory Techn.*, vol. 61, no. 8, pp. 3072–3082, Aug. 2013.

[44] M. Yajima and T. Hasegawa, "Beam pointing error of wideband planar phased array antennas with reduced True-Time-Delay devices," in *Proc. IEEE Int. Conf. Commun.*, vol. 9, Jun. 2006, pp. 4161–4166.

[45] G. Li, H. Zhao, and H. Hui, "Beam squint compensation for hybrid precoding in millimetre-wave communication systems," *Electron. Lett.*, vol. 54, no. 14, pp. 905–907, Jul. 2018.

[46] D. Zhang, Y. Wang, X. Li, and W. Xiang, "Hybridly connected structure for hybrid beamforming in mmWave massive MIMO systems," *IEEE Trans. Commun.*, vol. 66, no. 2, pp. 662–674, Feb. 2018.

[47] S. K. Garakoui, E. A. M. Klumperink, B. Nauta, and F. E. van Vliet, "Phased-array antenna beam squinting related to frequency dependency of delay circuits," in *Proc. 41st Eur. Microw. Conf.*, Oct. 2011, pp. 1304–1307.

[48] V. Venkateswaran and A.-J. van der Veen, "Analog beamforming in MIMO communications with phase shift networks and online channel estimation," *IEEE Trans. Signal Process.*, vol. 58, no. 8, pp. 4131–4143, Aug. 2010.

[49] F. Sohrabi and W. Yu, "Hybrid beamforming with finite-resolution phase shifters for large-scale MIMO systems," in *Proc. IEEE 16th Int. Workshop Signal Process. Adv. Wireless Commun. (SPAWC)*, Jun. 2015, pp. 136–140.

[50] J.-C. Chen, "Hybrid beamforming with discrete phase shifters for millimeter-wave massive MIMO systems," *IEEE Trans. Veh. Technol.*, vol. 66, no. 8, pp. 7604–7608, Aug. 2017.

[51] C. He, X. Liang, B. Zhou, J. Geng, and R. Jin, "Space-division multiple access based on time-modulated array," *IEEE Antennas Wireless Propag. Lett.*, vol. 14, pp. 610–613, 2015.

[52] Z. D. Zaharis, I. P. Gravas, P. I. Lazaridis, T. V. Yioultsis, C. S. Antonopoulos, and T. D. Xenos, "An effective modification of conventional beamforming methods suitable for realistic linear antenna arrays," *IEEE Trans. Antennas Propag.*, vol. 68, no. 7, pp. 5269–5279, Jul. 2020.

[53] G. M. Rebeiz, *RF MEMS: Theory, Design, and Technology*. Hoboken, NJ, USA: Wiley, 2004.

[54] C. A. Balanis, *Antenna Theory: Analysis and Design*. Hoboken, NJ, USA: Wiley, 2016.

[55] H. L. Van Trees, *Optimum Array Processing: Part IV Detection, Estimation, Modulation Theory*. Hoboken, NJ, USA: Wiley, 2004.

[56] S. K. Garakoui, E. A. M. Klumperink, B. Nauta, and F. E. van Vliet, "Time delay circuits: A quality criterion for delay variations versus frequency," in *Proc. IEEE Int. Symp. Circuits Syst.*, May 2010, pp. 4281–4284.

[57] J. A. Kong, *Electromagnetic Wave Theory*. Hoboken, NJ, USA: Wiley, 1986.

[58] W. Sierpinski, "Sur une courbe cantorienne qui contient une image biunivoque et continue de toute courbe donné," *CR Acad. Sci. Paris*, vol. 162, pp. 629–632, 1916.

[59] R. K. Mongia and P. Bhartia, "Dielectric resonator antennas—A review and general design relations for resonant frequency and bandwidth," *Int. J. Microw. Millim.-Wave Comput.-Aided Eng.*, vol. 4, no. 3, pp. 230–247, Jul. 1994.

[60] Y.-M. Pan, K. W. Leung, and K.-M. Luk, "Design of the millimeter-wave rectangular dielectric resonator antenna using a higher-order mode," *IEEE Trans. Antennas Propag.*, vol. 59, no. 8, pp. 2780–2788, Aug. 2011.

[61] Y. M. Pan, K. W. Leung, and K. Lu, "Omnidirectional linearly and circularly polarized rectangular dielectric resonator antennas," *IEEE Trans. Antennas Propag.*, vol. 60, no. 2, pp. 751–759, Feb. 2012.

[62] S. Rangan, T. S. Rappaport, and E. Erkip, "Millimeter-wave cellular wireless networks: Potentials and challenges," *Proc. IEEE*, vol. 102, no. 3, pp. 366–385, Mar. 2014.

[63] T. S. Rappaport, J. N. Murdock, and F. Gutierrez, "State of the art in 60-GHz integrated circuits and systems for wireless communications," *Proc. IEEE*, vol. 99, no. 8, pp. 1390–1436, Aug. 2011.

[64] H. S. C. Wang, "Performance of phased array antennas under error conditions," in *Proc. IEEE Aerosp. Appl. Conf.*, Feb. 1989, p. 25.

[65] H. S. C. Wang, "Performance of phased-array antennas with mechanical errors," *IEEE Trans. Aerosp. Electron. Syst.*, vol. 28, no. 2, pp. 535–545, Apr. 1992.

[66] B.-K. Yeo and Y. Lu, "Array failure correction with a genetic algorithm," *IEEE Trans. Antennas Propag.*, vol. 47, no. 5, pp. 823–828, May 1999.

[67] M. Levitas, D. A. Horton, and T. C. Cheston, "Practical failure compensation in active phased arrays," *IEEE Trans. Antennas Propag.*, vol. 47, no. 3, pp. 524–535, Mar. 1999.

[68] W. P. M. N. Keizer, "Element failure correction for a large monopulse phased array antenna with active amplitude weighting," *IEEE Trans. Antennas Propag.*, vol. 55, no. 8, pp. 2211–2218, Aug. 2007.

[69] A. A. M. Saleh and R. Valenzuela, "A statistical model for indoor multipath propagation," *IEEE J. Sel. Areas Commun.*, vol. 5, no. 2, pp. 128–137, Feb. 1987.

[70] R. Hu, J. Tong, J. Xi, Q. Guo, and Y. Yu, "Matrix completion-based channel estimation for mmWave communication systems with array-inherent impairments," *IEEE Access*, vol. 6, pp. 62915–62931, 2018.

CHUNGUO LI (Senior Member, IEEE) received the bachelor's degree in wireless communications from Shandong University, in 2005, and the Ph.D. degree in wireless communications from Southeast University, in 2010. In July 2010, he joined the Faculty of Southeast University, Nanjing China, where he became an Associate Professor, in 2012, an Advisor of Ph.D. candidates, in 2016, and a Full Professor, in 2017. From June 2012 to June 2013, he was the Postdoctoral Researcher with Concordia University, Montreal, Canada. From July 2013 to August 2014, he was with the DSL Laboratory, Stanford University, as a Visiting Associate Professor. From August 2017 to July 2019, he was an Adjunct Professor with Xizang Minzu University under the supporting Tibet Program organized by the China National Human Resources Ministry. He is an IET Fellow and the IEEE CIS Nanjing Chapter Chair. His research interests include wireless communications and cyberspace security, and machine learning-based image/video signal processing.

MENG HUA (Student Member, IEEE) received the B.S. degree in electrical and information engineering from Huangshan University, Huangshan, China, in 2013, and the M.S. degree in electrical and information engineering from the Nanjing University of Science and Technology, Nanjing, China, in 2016. He is currently pursuing the Ph.D. degree in information and communication engineering with the School of Information Science and Engineering, Southeast University, Nanjing. His current research interests include massive MIMO, energy-efficient wireless communication, UAV, mobile edge computing, and optimization theory.

WEN YAN (Member, IEEE) received the B.S. degree in electrical engineering from Tsinghua University, Beijing, China, in 2013. He is currently pursuing the Ph.D. degree in information and communication engineering with the School of Information Science and Engineering, Southeast University, Nanjing, China. From 2017 to 2018, he was a Visiting Ph.D. Student with the University of Wisconsin–Madison, Madison, WI, USA. His current research interests include statistical machine learning, graph mining, recommendation systems, and autonomous vehicle control.

LUXI YANG (Senior Member, IEEE) received the M.S. and Ph.D. degrees in electrical engineering from Southeast University, Nanjing, China, in 1990 and 1993, respectively. Since 1993, he has been with the Department of Radio Engineering, Southeast University, where he is currently a Professor of information systems and communications and the Director of the Digital Signal Processing Division. His current research interests include signal processing for wireless communications, MIMO communications, cooperative relaying systems, and statistical signal processing. He is the author or coauthor of two published books and more than 100 journal articles, and holds seven patents. He received the first- and second-class prizes of Science and Technology Progress Awards of the State Education Ministry of China, in 1998 and 2002. He has been the Vice Editor-in-Chief of the *Journal of Data Acquisition and Processing* (in Chinese), since 2007, and an Associate Editor of *Signal Processing* (in Chinese), since 2005. He is currently a member of Signal Processing Committee of Chinese Institute of Electronics.

XIAOLIANG PAN received the B.E. degree from Hohai University, Nanjing, China, in 2006, and the M.E. degree from the Nanjing University of Posts and Telecommunications, Nanjing, in 2011. He is currently pursuing the Ph.D. degree with the School of Information Science and Engineering, Southeast University, Nanjing. His current research interests include millimeter-wave communications and array signal processing.